1   # Superior colliculus visual neural sensitivity at the lower
2   # limit of natural self-induced image displacements
3
4   Ziad M. Hafed[1, 2], Chih-Yang Chen[1, 2, 3], and Fatemeh Khademi[1, 2]
5
6   1. Werner Reichardt Center for Integrative Neuroscience,
7   University of Tübingen, Tübingen, Germany
8   2. Hertie Institute for Clinical Brain Research,
9   University of Tübingen, Tübingen, Germany
10 3. Institute for the advanced study of Human biology (WPI-ASHBi), Kyoto University, Kyoto, Japan
11
12
13 **Correspondence to:**
14   Ziad M. Hafed
15   Werner Reichardt Center for Integrative Neuroscience
16   Otfried-Müller Str. 25
17   Tübingen, Germany, 72076
18   Tel: +49 7071 29 88819
19   Email: ziad.m.hafed@cin.uni-tuebingen.de
20
21
22

Abstract

Visual pattern analysis relies on computations from neurons possessing spatially confined receptive fields. Often, such receptive fields are orders of magnitude larger than the visual pattern components being processed, as well as these components' minute displacements on the retina, whether due to small object or self motions. Yet, perception effortlessly handles such visual conditions. Here, we show that in the primate superior colliculus, a brain structure long associated with oculomotor control, neurons with relatively large receptive fields are still sensitive to visual pattern displacements as small as 1 min arc. We used real-time gaze-contingent retinal image stabilization to control the instantaneous spatio-temporal luminance modulation of detailed patterns experienced by neurons, probing sensitivity to the lower limit of natural self-induced image displacements. Despite a large difference between pattern displacement amplitudes and receptive field sizes, collicular neurons were strongly sensitive to the visual pattern consequences of the smallest possible image-shifting eye movements.

Introduction

Image analysis in the primate visual system is performed by neurons having individual receptive fields (RF's) sampling confined regions of the retinal image. Outside the fovea, and particularly in higher visual areas, RF's can be large. This is also the case in sensory-motor structures like the superior colliculus (SC) [1-3], which itself has a rich and diverse visual repertoire [1-7].

Integration of relatively large image regions by individual RF's raises questions about how detailed visual pattern analysis can occur when the local features inside an RF are much smaller than RF size. Among these questions is what nature of visual processing takes place in the SC, a sensory-motor structure, when compared to other visual areas that are more distant from the motor control apparatuses. For example, the SC contributes to saccade generation [8], and its diverse visual properties seem to be optimized for detecting stimuli for the purpose of gaze orienting [9]. Does this mean that SC neurons are incapable of detailed visual pattern analysis that may be more the purview of visual cortex?

We investigated this question by exploring whether SC neurons are sensitive to the visual pattern consequences of minute image displacements over their RF's. With the head fixed, a lower limit on natural self-induced retinal image motion is that caused by slow ocular position drifts during gaze fixation (Fig. 1A) [10-12]. With stable external stimuli, such drifts introduce image pattern displacements over individual RF's that are much smaller than the RF's themselves (Fig. 1B). Thus, the local pattern features of the stimuli never really leave the RF's during drifts. Yet, theoretical and perceptual work suggests that small displacements associated with ocular position drifts reformat images in meaningful ways for perception [13-16]. The reformatting itself is a direct consequence of eyeball rotation: it is a property of the image formation process. However, for the reformatting to be effective for perception, downstream neural processing stages need to be also sensitive to them. Therefore, we asked whether SC neurons functionally utilize the visual reformatting afforded by ocular position drifts in their activity (Fig. 1B).

We employed the technique of gaze-contingent retinal image stabilization, combined with grating images of different properties, to identify a direct SC neural correlate of perceptual effects [13] associated with ocular position drifts. We presented gratings to the RF's of SC neurons either stably on the display (and thus moving on the retina due to drifts) or using gaze-contingent display updates, as was done earlier in the primary visual cortex with simple spot and bar stimuli [17]. We used, instead, patterned gratings and different experimental manipulations of retinal image motions to demonstrate clear SC neural sensitivity (even extrafoveally) to the diminutive visual pattern consequences of ocular position drifts. These results complement studies in the retina highlighting the impact of visual reformatting by drifts on the retinal output [18], and they demonstrate that SC neurons can contribute to visual scene analysis with high fidelity despite their relatively large RF's.

Results

We asked whether visually-responsive SC neurons are sensitive to image pattern displacements at the lower limit of natural self-induced motion. We did so by recording SC neural activity from head-fixed monkeys precisely holding their gaze on a small, stable fixation spot of 8.5 x 8.5 min arc dimensions. During fixation, the eyes drifted slowly [10-12], causing retinal image displacements on the order of 1 min arc magnitude (Fig. 1A), with occasional larger microsaccades. The scale of retinal image displacements associated with ocular position drifts, as small as the approximate distance between two individual foveal cone photoreceptors, is considerably smaller than SC RF sizes, especially extrafoveally [1-3,9]. It is also frequently much smaller than the viewed image patterns themselves. Consider, for example, a gabor grating of 4.44 cycles/deg (cpd) in an RF of a neuron preferring 3.5 deg eccentricity. A displacement over the RF of the grating's retinal image by 1 min arc would cause minimal change to the overall luminance pattern experienced by the neuron (Fig. 1B). Yet, theoretical considerations suggest that such minute pattern displacements can still matter for perception [10,13-16]. We, therefore, investigated whether SC neurons are sensitive to these diminutive pattern displacements.
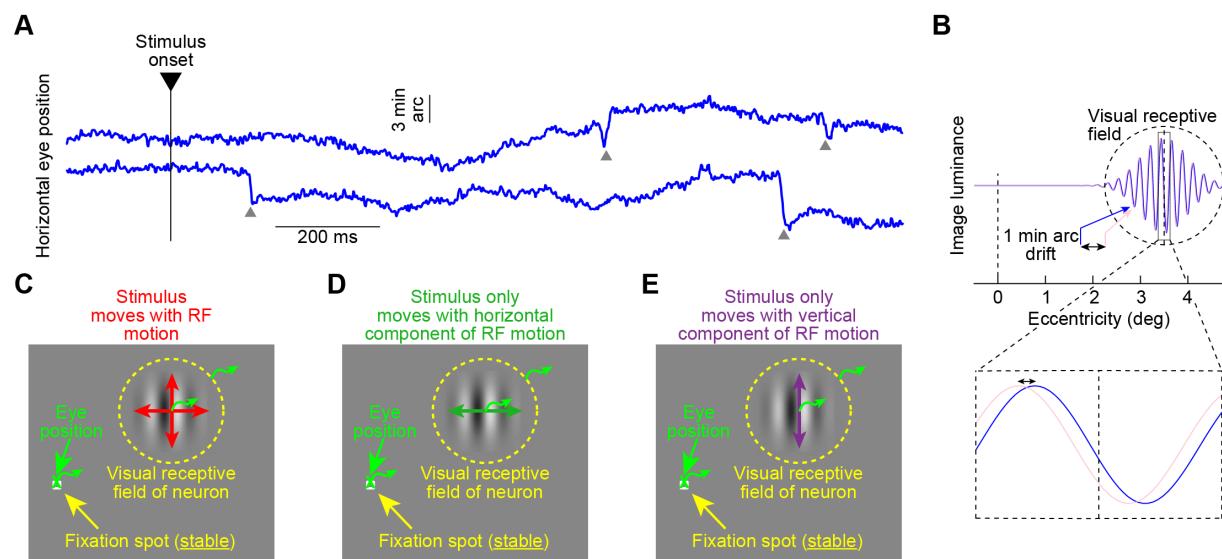

Figure 1 Isolating the visual-pattern consequences of slow eye position drifts on SC neural activity. (A) Horizontal eye position from two example gaze fixation trials. Microsaccades are highlighted with arrows and were removed from all analyses (Methods). In between, slow eye position drifts occurred with a retinal-image displacement range on the order of 1-3 min arc. **(B)** The luminance profile of a 4.44 cpd gabor grating placed within a visual receptive field (RF) of a hypothetical SC neuron for two instantaneous eye positions separated by 1 min arc (blue versus pink; the bottom inset magnifies one cycle). The image displacement is much smaller than the RF size (depicted based on our prior measurements [3,9]). **(C)** To characterize SC neural sensitivity to pattern displacements on the order of 1-3 min arc, we exploited the slow position drifts in **A**. Monkeys fixated a stable spot, and we continuously translated the image of an eccentric grating with fixational eye motion, thus stabilizing the grating's image within the continuously moving retinotopic RF. This minimized the displacements of the grating in the RF that would have otherwise occurred. **(D)** In other conditions, we only stabilized the horizontal component of ocular position changes (minimizing RF image shifts orthogonal to the grating). **(E)** In yet other conditions, we only stabilized the vertical component of eye drift. Curly bright green arrows in **C, D, E** schematize the eye position changes and their associated retinotopic RF motions.

125
126
127   We utilized real-time retinal image stabilization to move a visual pattern (gabor grating) in
128   lock with instantaneous eye position (Methods). We compared neural activity with a stable
129   pattern on the display (thus moving with respect to a continuously moving retinotopic RF) to
130   neural activity with a moving pattern on the display tracking the eye movements (and thus
131   rendered more stable with respect to the RF; Fig. 1C). If the SC is sensitive to visual pattern
132   consequences of retinal image displacements as small as those in Fig. 1A, B, then the neural
133   responses should differ between the two conditions. Critically, the fixation spot was always
134   stable on the display, allowing the monkeys to properly anchor their gaze independently of
135   retinal image stabilization. Indeed, the characteristics of both ocular position drifts and
136   microsaccades across all of our gaze-contingent manipulations (Methods) were unaltered by
137   whether the grating was stable on the display (control) or not (Figs. S1-S3). This is consistent
138   with evidence that, in steady-state fixation, microsaccades and ocular position drifts act to
139   optimize eye position at the fixated target [19-22]. Therefore, we experimentally controlled the
140   subtle image displacements of visual patterns over RF's (Fig. 1), but without altering the
141   natural gaze behavior itself.
142
143
144   *Superior colliculus neurons are sensitive to visual pattern displacements on the*
145   *order of 1 min arc*
146   We first established the effectiveness of our manipulation. After identifying a visually-
147   responsive neuron, we estimated its retinotopic RF hotspot location and extent (Methods). If
148   we then pegged the stimulus, via retinal image stabilization, at the estimated hotspot
149   location, then the neuron would consistently experience an optimal stimulus. This is in
150   contrast to control trials, during which fixational eye movements could, at any one moment
151   in time, displace the stimulus from the optimal RF hotspot location or otherwise blur it.
152   Thus, neural activity was expected to be elevated with retinal image stabilization (Fig. 2).
153   Alternatively, if we pegged the stimulus at a sub-optimal location relative to the RF during
154   retinal image stabilization, then the neuron's activity was expected to decrease, because in
155   control trials, eye movements could momentarily bring the stimulus to a more optimal RF
156   position (Fig. S4). These effects are similar to those observed in V1 with the retinal image
157   stabilization technique and simple spot and bar stimuli [17,23,24], and they meant that we were
158   now in a good position to explore, in more detail, the visual pattern consequences of minute
159   ocular position drifts on SC image representations.
160
161   In all of our subsequent analyses, we only focused on situations like in Fig. 2, with an
162   optimally placed RF stimulus, and also with primarily extrafoveal neurons with RF's larger
163   than the scale of ocular position drifts; this was the relevant scenario for the questions
164   raised by Fig. 1B. We also excluded all epochs around microsaccades (Methods), because
165   retinal image stabilization with discretized display update times (Methods) is expectedly [17]
166   least effective for these faster eye movements (but see Fig. S5 for evidence of the
167   effectiveness of the technique in tracking eye motions even with microsaccades).
168
169
170
171
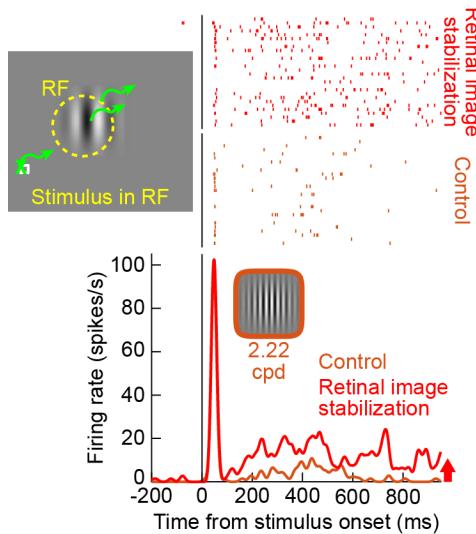
172
173
174 **Figure 2 Example SC neuron illustrating the effect of retinal image stabilization on SC activity.** In control trials,
175 we presented a grating of middle spatial frequency (2.22 cpd) near RF center. The neuron had a weak response
176 after the initial visual burst. In retinal image stabilization trials, we continuously updated the position of the
177 grating with fixational eye position (predominantly ocular drift; Fig. 1A), to render the grating's retinotopic
178 position relative to the RF more stable than in control trials. The neuron's sustained visual response was
179 significantly elevated, suggesting that smearing of the grating position over the RF in control trials reduced the
180 overall responsiveness of the neuron. Our analyses focused on sustained responses, to avoid the transients
181 associated with stimulus onsets at the beginnings of trials (Methods). Fig. S4 also shows an additional validation
182 of the stabilization technique, this time when placing the grating away from the RF center of a recorded neuron.

183
184
185
186
187 Retinal image stabilization of a stimulus at the RF hotspot location consistently elevated SC
188 neural activity, suggesting sensitivity to local image pattern statistics within the RF's (like
189 those schematized in Fig. 1B). In Fig. 3A, we plotted the normalized population activity after
190 the onset of a 4.44 cpd grating in the RF's, either in control or with full retinal image
191 stabilization. We found a persistently elevated sustained response (after an initial visual
192 burst due to stimulus onset) for as long as the stimulus was stabilized over the RF's (compare
193 control to retinal image stabilization firing rates). Given the spatial scale of our image
194 displacements associated with ocular position drifts and the predicted luminance
195 modulations that they introduced (Figs. 1A, S1, S3C-F), this implies that SC neurons can
196 indeed detect minute image pattern displacements much smaller than RF sizes, and also
197 smaller than the pattern features themselves (Fig. 1B). Figure 3B also shows the distribution
198 of individual neural modulation indices (Methods) across our population, with a significant
199 positive shift indicating consistently elevated firing rates during retinal image stabilization
200 (21.74% average modulation index relative to control; $p=3.2073 \times 10^{-8}$; 1-sample t-test; n=61
201 neurons). Moreover, Fig. S6A shows the individual neuron raw firing rates during sustained
202 fixation (shaded gray region on the x-axis of Fig. 3A, and excluding microsaccades) in the two
203 conditions: practically all neurons exhibited elevated activity for vertical 4.44 cpd gratings
204 stabilized over their RF's as opposed to being jittered by ocular position drifts in the control
205 condition. This is a direct SC neural correlate of the concept of temporal encoding by ocular
206 position drifts predicted theoretically [13-15], but now being viewed from the individual neuron
207 perspective.
208

209
210
211
212
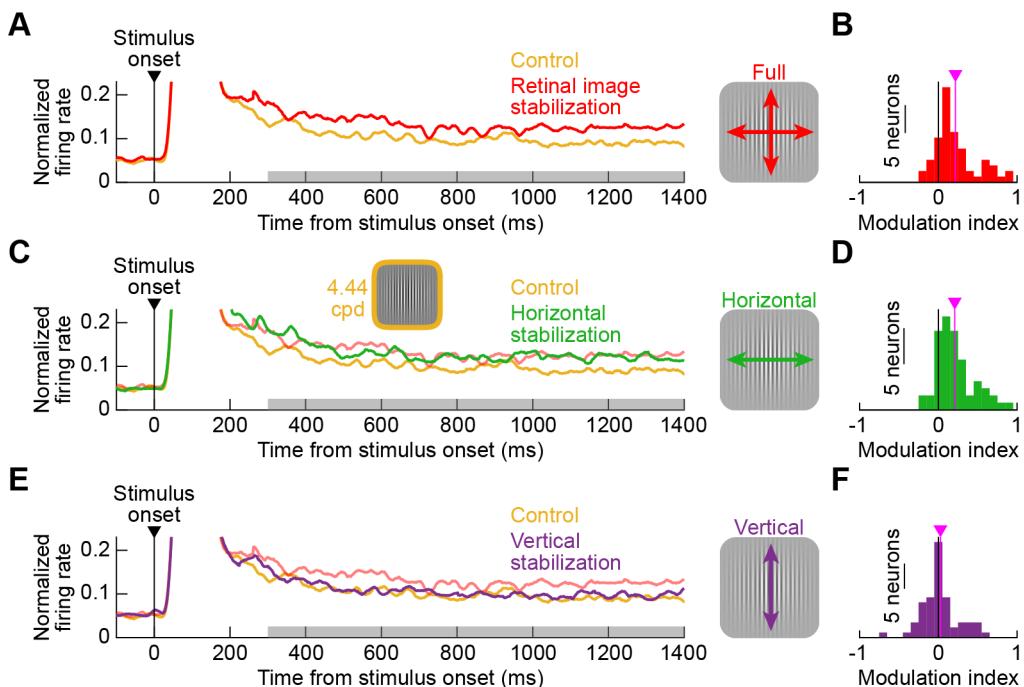
213
214
215 **Figure 3 SC neurons are sensitive to image pattern displacements as small as 1-3 min arc in amplitude. (A)**
216 Normalized firing rate across our population after the onset of a 4.44 cpd grating in the RF's. Yellow shows the
217 control condition in which the grating was stable on the display, and therefore continuously being displaced over
218 the retinotopic RF's. The neurons exhibited a sustained response above baseline, as long as there was a stimulus
219 presented. Red shows the full retinal image stabilization condition (Fig. 1C), in which the firing rate was
220 persistently elevated. The gray horizontal bar on the x-axis defines our measurement interval for our analyses
221 (Methods). **(B)** Distribution of per-neuron modulation indices comparing the sustained response under full
222 retinal image stabilization to the sustained response in control (Methods). The vertical pink line shows the mean
223 modulation index across the population (individual neuron raw measurements are also shown in Fig. S6A). **(C)**
224 Same as **A** but for retinal image stabilization of only the horizontal component of eye position displacements
225 (orthogonal to the grating orientation). The neurons were as affected as in the full retinal image stabilization
226 condition (the faint red curve is replicated from **A** for easier comparison). This is because a vertical ocular position
227 drift over a vertical grating causes no luminance modulations over the RF's beyond the original image pattern.
228 **(D)** Modulation index distribution for the data in **C**, showing similar effects to full retinal image stabilization. **(E)**
229 With vertical retinal image stabilization, the neurons were unaffected by the gaze-contingent image
230 manipulation: the horizontal component of RF motion relative to the grating was the same as in control, resulting
231 in the same neural response. **(F)** Modulation indices for vertical retinal image stabilization were not significantly
232 different from zero across the population.

233
234
235

Drift-scale pattern displacements orthogonal to the patterns' orientations drive
neural modulations the most

238 The results of Fig. 3A, B might have been an artifact of world-centered grating motion, which
239 was necessarily introduced by retinal image stabilization (by stabilizing the retinal image, we
240 had to move the stimulus on the display). We, therefore, tested the stronger predictions
241 afforded by either horizontal or vertical retinal image stabilization (Fig. 1D, E). Here, with the
242 same vertical 4.44 cpd grating, if we stabilized only the horizontal component of fixational

7

243 eye movements, then any residual vertical movements of the grating over the retinotopic
244 RF's (uncompensated by the partial gaze-contingent technique) would not alter the
245 luminance pattern over the RF's too much; this is because the vertical component of ocular
246 position drifts is much smaller than the grating size and also parallel to it (Fig. 1D). On the
247 other hand, if we stabilized only the vertical component of fixational eye movements (Fig.
248 1E), then the residual (uncompensated) horizontal movements of the grating over the
249 retinotopic RF's would cause luminance pattern changes like in Fig. 1B. More importantly,
250 since the ocular position drift statistics were unchanged across all of our manipulations (Fig.
251 S1, S3C-F), the residual horizontal motions experienced by the neurons would be highly
252 similar to those in the control condition, as if there was no retinal image stabilization at all.
253 Thus, at the individual neural modulation level, horizontal retinal image stabilization should
254 look indistinguishable from full retinal image stabilization relative to the control condition,
255 and vertical retinal image stabilization should appear like the control condition instead; this
256 is despite both conditions causing world-centered grating motions on the display.
257
258 Our neurons were modulated according to the predictions of retinotopic pattern
259 displacements over the RF's (Fig. 1B-E), suggesting sensitivity to local features much smaller
260 than SC RF size. During horizontal retinal image stabilization, the neurons' activity was
261 elevated as much as in full retinal image stabilization (Fig. 3C, D; average modulation index
262 20.86%; significantly larger than zero; p=7.8757x10^{-9}; 1-sample t-test; n=61 neurons). On the
263 other hand, the neurons' firing rates were unchanged from control with vertical retinal
264 image stabilization (Fig. 3E, F; population modulation index not significantly different from
265 zero; p=0.3898; 1-sample t-test; n=61 neurons). The difference between horizontal and
266 vertical retinal image stabilization was also robustly evident at the individual neuron level
267 (Fig. S6B), and the spiking statistics in the two conditions mimicked those in either full retinal
268 image stabilization (for the case of horizontal stabilization; Fig. S6C) or control (for the case
269 of vertical stabilization; Fig. S6C). Therefore, SC neurons are sensitive to the image pattern
270 displacements associated with ocular position drifts, despite the small scale of such drifts
271 (and the local image features) relative to RF size. This means that SC neurons with relatively
272 large RF's can benefit from the edge enhancing properties of ocular position drifts seen
273 perceptually [13].
274
275 To further demonstrate the sensitivity of SC neurons to minute pattern displacements
276 orthogonal to the local edges in the patterns, we also repeated the same experiments in one
277 monkey but with horizontal, rather than vertical, 4.44 cpd gratings. Thus, in this monkey, we
278 could test some neurons under two different pattern conditions within the same session
279 (Methods). With vertical gratings, we replicated the results of Fig. 3, as seen in Fig. 4A, B.
280 With horizontal gratings (Fig. 4C, D), it was now vertical retinal image stabilization (as well as
281 full stabilization) that resulted in the largest neural modulations; horizontal stabilization
282 (parallel to the now horizontal gratings) caused the least modulations (also see Fig. S7
283 showing individual neuron firing rates as well as spiking statistics in the different conditions).
284 Thus, it was always ocular position drifts orthogonal to the local pattern orientations that
285 resulted in the largest neural modulations.
286
287 Therefore, not only are SC neurons sensitive to image pattern displacements on the order of
288 magnitude of 1 min arc, but they are also differentially sensitive as a function of the relative
289 difference between the image displacement directions and the underlying pattern
290 orientations. We previously demonstrated this to be the case in the SC for the image

291   displacements associated with significantly larger microsaccades [25], but the smaller scale of
292   ocular position drifts (Fig. 1A, B) suggests an even finer ability of SC neurons to represent
293   and react to detailed visual patterns (Fig. 1B). The SC can indeed contribute to the
294   theoretically-predicted perceptual effects associated with slow ocular position drifts (e.g.
295   [13,15]).

296
297
298
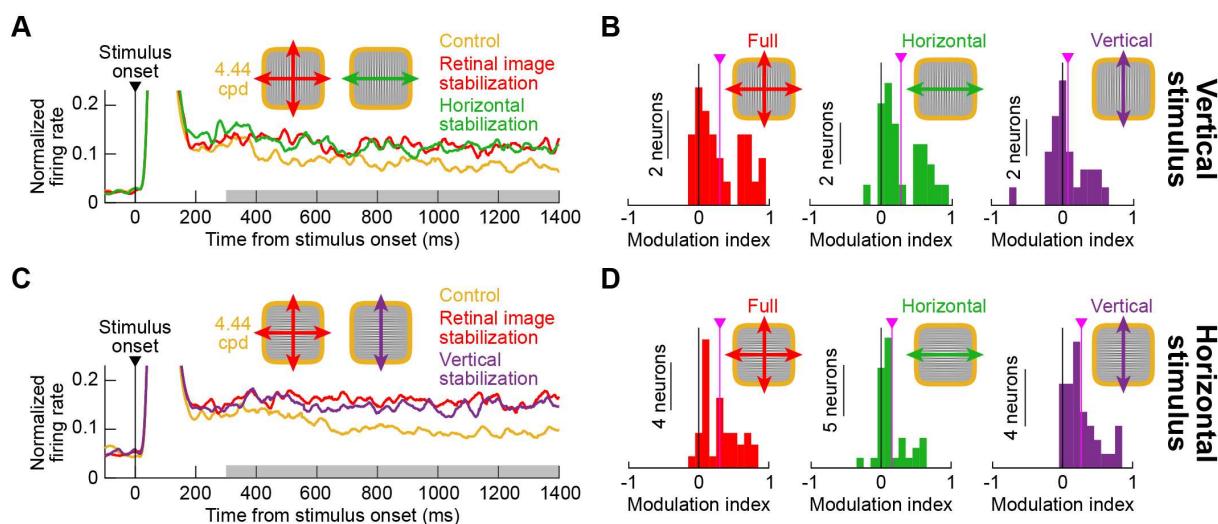
299
300
301 **Figure 4 Ocular position drifts orthogonal to a pattern cause the biggest neural modulations, independent of**
302 **original pattern orientation. (A, B)** Neural modulations similar to Fig. 3 from a monkey viewing a vertical 4.44
303 cpd grating. Full and horizontal (orthogonal to the grating orientation) retinal image stabilization caused the
304 biggest neural effects. The modulation indices for vertical retinal image stabilization (rightmost histogram in **B**)
305 were not significantly different from zero (p=0.1728; 1-sample t-test; n=27); the indices were significant for full
306 (p=6.741x10^{-5}) and horizontal (p=3.854x10^{-5}) stabilization (left and middle histograms in **B**). **(C, D)** SC neural
307 activity modulations in the same monkey viewing a horizontal grating instead of a vertical one. Now, horizontal
308 retinal image stabilization had the weakest effect (middle histogram in **D**; 15.56% modulation; p=1.1x10^{-4}; 1-
309 sample t-test; n=35). Vertical retinal image stabilization resulted in similar neural modulations to full retinal
310 image stabilization (26.84% and 30.14%, respectively, in the rightmost and leftmost histograms in **D**; both
311 significantly different from zero: p=1.1x10^{-7} and 4.1x10^{-8}). All other conventions similar to Fig. 3. Also see Fig. S7
312 for individual neuron results.

313
314
315
316

317 *Neural responses to high spatial frequency patterns are modulated the most by*
318 *drift-scale image displacements*
319 The results so far suggest that SC neurons are sensitive to image pattern features that can be
320 significantly smaller than the neurons' RF sizes (Fig. 1B). However, with a pattern at the
321 optimal RF location, the scale of luminance modulations caused by ocular position drifts (Fig.
322 1B) should depend on both the spatial detail of the pattern itself as well as the spatial scale
323 of the retinal image displacements caused by eye movements (Fig. S3A, B). Therefore, given
324 the ocular position drift sizes that we observed (Figs. 1A, S1, S3C-F), we expected to observe
325 the largest effects of retinal image stabilization with high spatial frequency patterns (Fig.
326 S3A, B). This was indeed the case. In our experiments, we also tested low (0.56 cpd) and
327 intermediate (2.22 cpd) spatial frequency gratings (Methods). For both vertical (Fig. 5) and
328 horizontal (Fig. S8) gratings, the relevant orthogonal stabilization condition (horizontal in Fig.

329   5 and vertical in Fig. S8) resulted in the largest neural modulation indices for 4.44 cpd
330   gratings. For example, with vertical gratings and horizontal stabilization, the average
331   modulation index with 4.44 cpd was 20.86% relative to control, but it was 12.46% for 0.56
332   cpd (p=0.0319; 2-sample t-test; n=61 neurons; comparing 4.44 cpd to 0.56 cpd; Fig. 5B); the
333   modulation index was 13.27% for 2.22 cpd (p=0.0997; 2-sample t-test; n=61 neurons;
334   comparing 4.44 cpd to 2.22 cpd; Fig. 5C). Naturally, full retinal image stabilization also
335   showed similar effects to orthogonal image stabilization, as expected from Figs. 3, 4.
336   Therefore, SC neurons are lawfully sensitive to the luminance modulations caused by
337   orthogonal edges being displaced ever so slightly within their RF's due to ocular position
338   drifts.

339
340
341
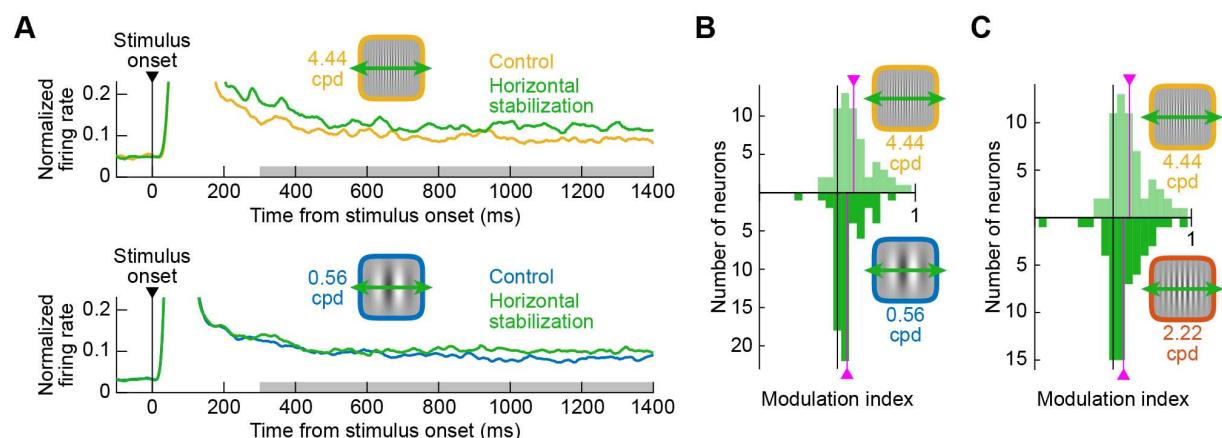
344 **Figure 5 The representation of high spatial frequency features in the SC is most sensitive to the smallest**
345 **naturally-induced image displacements. (A)** Normalized population firing rates in control and with horizontal
346 retinal image stabilization for 4.44 cpd (top) and 0.56 cpd (bottom) vertical gratings. The high spatial frequency
347 grating was associated with a larger neural modulation than the low spatial frequency grating (consistent with
348 the image luminance predictions of Fig. S3A, B). **(B)** Neural modulation indices comparing high (top) and low
349 (bottom) spatial frequencies with horizontal retinal image stabilization (pink vertical lines indicate the mean
350 across the population). The high spatial frequency grating was associated with higher modulation indices. **(C)**
351 When comparing the high to the middle spatial frequency, the difference in modulation indices was smaller than
352 in **B** (but the modulation indices with 4.44 cpd were still higher than with 2.22 cpd; 20.86% versus 13.27%).

353
354
355

356 *Sensitivity to drift-scale pattern displacements still occurs in extrafoveal and*
357 *lower visual field neurons with larger receptive fields*
358 In prior theoretical and perceptual work [13,15], the image pattern consequences of ocular
359 position drifts were primarily, and understandably, considered from a foveal perspective.
360 However, our results above suggest that even eccentricities with larger RF's (Fig. 1B) may
361 still utilize the visual formatting afforded by slow fixational eye movements in SC visual
362 neural coding. Therefore, we exploited the fact that we sampled neurons from a wide range
363 of eccentricities (Fig. S9), and we specifically analyzed extrafoveal neurons to ask if they
364 were still sensitive to our retinal image stabilization manipulations. These extrafoveal SC
365 neurons clearly showed modulations (Fig. 6A) that were very similar to those observed for
366 the entire neural population (Figs. 3-5): greater elevation with retinal image stabilization for
367 high than low spatial frequencies.

368
369 We then separated the neurons into 3 groups based on their preferred eccentricities (<1
370 deg, 1-3 deg, and >3 deg). In all cases, full and horizontal retinal image stabilization (with
371 vertical gratings) had higher positive neural modulation indices than vertical retinal image
372 stabilization (Fig. 6B). Specifically, the full and horizontal retinal image stabilization
373 modulation indices in Fig. 6B were statistically significantly different from zero (p<0.0026 in
374 each panel; 1-sample t-test; neuron numbers shown in Fig. 6B), but the vertical retinal image
375 stabilization modulation indices were not. Moreover, the modulation indices were higher for
376 high rather than low spatial frequencies (Fig. 6C); each comparison of high (4.44 cpd) to low
377 (0.56 cpd) spatial frequency modulation indices in Fig. 6C was statistically significant
378 (p<0.032 in each panel; 2-sample t-test; neuron numbers shown in Fig. 6C), except for >3
379 deg eccentricities (which still showed the same trends; p=0.1683). Thus, even extrafoveal SC
380 neurons with larger RF's are sensitive to the visual pattern consequences of ocular position
381 drifts on the order of magnitude of 1 min arc, and with the same dependencies as in Figs. 3-
382 5. It should also be noted that the effect sizes of retinal image stabilization were smaller with
383 the larger RF's (e.g. compare modulation indices across the three rows in Fig. 6B, C), which
384 might be due to the larger integration areas of the larger RF's in the periphery.
385
386
387
388
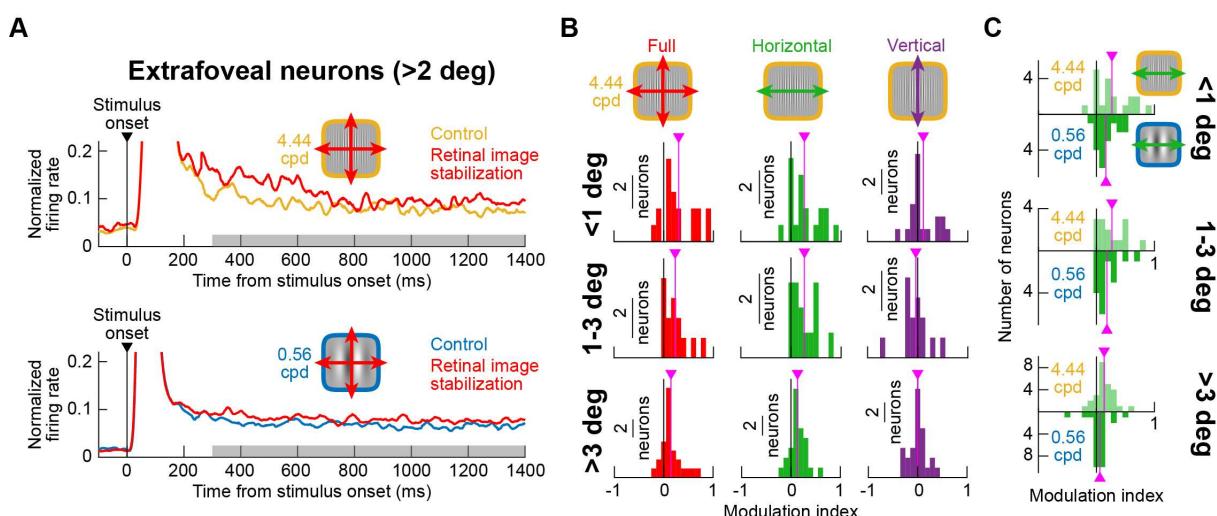
391 **Figure 6 Visual formatting of SC neural responses by ocular position drifts persists for extra-foveal neurons**
392 **with larger RF's. (A)** Normalized population firing rates from all extra-foveal SC neurons comparing control and
393 retinal image stabilization conditions for high (top) and low (bottom) spatial frequencies. Similar observations to
394 Figs. 3-5 could be made: there was still an effect of retinal image stabilization despite the larger RF's of extra-
395 foveal SC neurons (see also Fig. 1B). **(B)** Modulation indices as in Figs. 3, 4 for three different groups of neurons
396 according to their preferred eccentricities. Full and horizontal retinal image stabilization had positive modulation
397 indices across eccentricities, whereas vertical retinal image stabilization modulation indices were always closest
398 to zero. Note also that the modulation indices for full and horizontal retinal image stabilization progressively
399 decreased in amplitude with increasing eccentricities (top to bottom). **(C)** Modulation indices comparing high
400 and low spatial frequencies (as in Fig. 5) across the different groups of neurons. The same observations as in Fig.
401 5 were still made for extra-foveal SC neurons.
402
403
404

405   Another test of the effects of RF sizes in our retinal image stabilization manipulations was to
406   also check upper and lower visual field SC neurons. This is so because, in the very same
407   animals, we previously documented a substantial difference in SC RF sizes above and below
408   the horizontal meridian, with lower visual field RF's being significantly larger [9]. Here, we
409   found that even such lower visual field neurons, with significantly larger RF's than upper
410   visual field neurons [9], still showed all the same hallmarks of neural modulations described
411   above (Figs. S10, S11). Thus, visual reformatting of the SC neural code by slow ocular
412   position drifts extends well beyond the fovea and affects extrafoveal and lower visual field
413   neurons with larger RF's (Fig. 1B).
414
415

Neural modulatory effects of ocular position drifts still occur without
417   *experimental retinal image stabilization*
418   Finally, if SC neurons are indeed sensitive to the visual pattern consequences of ocular
419   position drifts, might it be possible to observe hallmarks of this even without retinal image
420   stabilization? To test this, we inspected our control trials in more detail. Since we did not
421   have experimental control over individual retinal image stimulation in this condition, we
422   picked, instead, microsaccade-free fixation epochs that were confined within a small eye
423   position window (+/- 3 min arc) in any given trial. We hypothesized that, with a vertical
424   grating, momentary epochs of microsaccade-free fixation with particularly large horizontal
425   eye position deviation within such a confined spatial window might drive a luminance
426   transient signal from the neurons more than epochs of low horizontal deviation (a kind of
427   momentary refreshing due to image translation, like with microsaccades [25] but on the much
428   smaller scale of ocular position drifts). For example, in Fig. 7A, we had two 250-ms
429   microsaccade-free epochs, with the left one showing a high deviation in horizontal eye
430   position during the first 200 ms and the right one showing a low deviation (Fig. 7B shows the
431   vertical eye position deviations from the same epochs). If we now measured neural activity
432   in the final 50 ms, assuming a temporal integration window of approximately 100-200 ms as
433   per prior measurements of the SC [26], then we might expect that the recent history of
434   luminance changes over the RF (in the past 200 ms) provides stronger sensory motion drive
435   from the large horizontal deviation epochs than the low horizontal deviation epochs (or any
436   vertical deviation epochs). In other words, refreshing of the image pattern representation in
437   the RF would be the largest (for a given retinal image position) with an orthogonal recent
438   shift of the pattern.
439

440   This was indeed the case. We divided all 250-ms microsaccade-free epochs, only from
441   control trials, into high or low horizontal deviation (while still maintaining the average
442   position of the retinal image of the grating within a confined spatial window; Methods),
443   according to the median deviation value in each session. With a vertical grating of 4.44 cpd,
444   the epochs with high horizontal deviation consistently resulted in higher firing rates in the
445   final 50 ms than the epochs with low horizontal deviation (Fig. 7C; $p=1.2\times10^{-4}$; 2-sample t-
446   test; n=61 neurons). When we repeated the same analysis based on epochs of large or small
447   vertical eye position deviations instead, there was no longer a difference (Fig. 7D; p=0.1688;
448   2-sample t-test; n=61). This is because vertical drift over a vertical grating caused minimal
449   image changes in the RF's, and it is consistent with our horizontal and vertical retinal image
450   stabilization results above (e.g. Figs. 3, 4). Similarly, with low, rather than high, spatial
451   frequency patterns, the effects were significantly diminished (Fig. 7E, F; p=0.445 for E and
452   p=0.8227 for F; 2-sample t-test; n=61 neurons), consistent with Fig. 5. Therefore, SC neurons

453 are sensitive to the visual pattern consequences of ocular position drifts even without any
454 physical stimulus motion on the display caused by our retinal image stabilization technique.
455
456
457
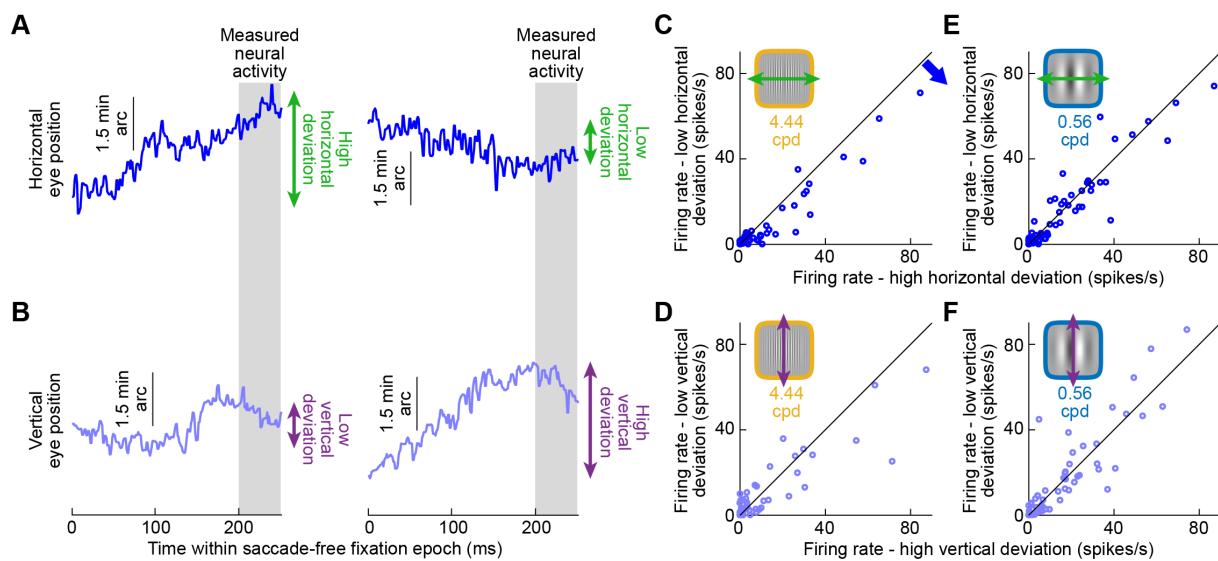
Figure 7 Naturally occurring ocular position drifts in the absence of experimental retinal image stabilization also significantly modulate the representation of high spatial frequency features in the SC. (A) Example microsaccade-free fixation epoch from two control trials (right and left) having either a large (left) or small (right) ocular position drift in the horizontal direction. We only picked epochs in which eye position remained within a confined spatial window despite the drift variations (Methods). **(B)** Vertical eye positions from the same two trials as in **A**. The epoch with high horizontal drift had low vertical deviation (left), and the epoch with low horizontal drift had high vertical deviation (right). **(C)** For all control trials with a high spatial frequency grating, we measured firing rate in a 50 ms interval (gray in **A, B**) preceded by a 200-ms microsaccade-free fixation epoch, and we divided the epochs as having a horizontal deviation larger (x-axis) or smaller (y-axis) than the median horizontal deviation across all epochs in a given neuron. Instantaneous firing rates preceded by a period of large horizontal position deviations (orthogonal to the vertical grating) were associated with systematically higher firing rates. **(D)** This effect was absent when assessing the impact of large and small vertical eye position drifts relative to the vertical gratings. **(E, F)** For a low spatial frequency grating, neither horizontal **(E)** nor vertical **(F)** drifts significantly modulated neural activity. For horizontal drifts, this is consistent with the sizes of eye position drifts relative to the gratings' luminance spatial profiles (Figs. 1, S3A, B). For vertical drifts, this is consistent with the lack of significant luminance modulation of the vertical pattern by a subtle vertical image displacement.

476
477
478

Discussion

We found that individual SC neurons, even with large RF's, are sensitive to minute displacements of visual patterns caused by ocular position drifts on the order of 1 min arc in amplitude. We were particularly motivated by the question of whether the diverse visual capabilities of the primate SC, which are becoming increasingly evident, include being sensitive to local feature patterns that are significantly smaller than the RF's themselves (Fig. 1B). Thus, we investigated whether subtle shifts of these patterns caused by ocular position drifts, representing the lower limit of natural self-induced image displacements, can reliably and systematically modulate SC neural activity. We employed retinal image stabilization to experimentally control the location and motion of a given pattern over the RF at any one moment in time. If the RF's grossly integrated information all over their spatial extents, then

491 subtle shifts of a given pattern (Fig. 1B) should not have resulted in altered neural responses.
492 In contrast, we found robust neural modulations, which were also direction-dependent.
493 Thus, even though SC neurons may have large RF's, they still exhibit sensitivity to highly local
494 image features. This idea is consistent with the notion that the primate SC can contribute to
495 visual scene analysis [4,5,26] and object processing [6,27-30] in a variety of ways.
496
497 Our results are relevant with respect to theoretical predictions on how eye position drifts
498 can reformat visual images by introducing temporal fluctuations of image luminance at any
499 one position on the retina [13-16,31]. Such image reformatting happens by virtue of a physical
500 rotation, albeit small, of the eyeball when viewing a stationary image. However, for such a
501 reformatting to actually influence perception in a meaningful way, then neural elements
502 downstream of the retina must be sensitive to its consequences. With small foveal RF's, say
503 in the lateral geniculate nucleus or primary visual cortex, this idea might be expected
504 because small ocular position drifts can displace stimuli in and out of the equally small RF's;
505 that is, the scale of image shifts is similar to the scale of foveal (and perifoveal) RF sizes.
506 However, whether larger RF's (e.g. extrafoveally), and particularly within an area that is
507 more traditionally investigated from the perspective of motor control like the SC, can still
508 benefit from such reformatting was not equally clear. We found this to be the case, adding
509 to the increasingly rich repertoire of visual capabilities of the primate SC described in the
510 literature. Thus, visual reformatting by ocular position drifts for the benefit of perception
511 can extend also beyond the fovea, and it has direct neural consequences downstream of the
512 retina.
513
514 An additional interesting implication of our results concerns the degree of correlation
515 between the two eyes during ocular position drifts. We experimentally stabilized our grating
516 images based on the motion of only one eye (Methods), and we still observed very
517 systematic neural modulations. This means that there must have been at least a minimal
518 amount of correlation between the motions of the two eyes. Otherwise, our retinal image
519 stabilization conditions would have created disparities between the left and right eye images
520 that might have blurred the gratings too much. This would not have necessarily increased
521 the gain and directional sensitivity of neural responses with retinal image stabilization like
522 we saw. Therefore, it will be important in future work to better investigate binocular
523 coordination in ocular position drifts during gaze fixation. Indeed, the question of whether
524 ocular position drifts are correlated (either positively or negatively) between the two eyes
525 has been investigated in the past, with a variety of observations and interpretations [12,32]. It
526 has also been previously shown that primates are capable of controlling slow eye
527 movements with speeds and position changes similar to those obtained with ocular position
528 drifts during fixation [20,33,34].
529
530 In yet additional future experiments, stabilization based on only one eye motion could be
531 exploited experimentally to investigate the strength of binocular and monocular visual input
532 integration in the SC. Specifically, it is known that most of the SC is binocular [1,35-37]. However,
533 it could be that some neurons' activity may be dominated by one eye input or the other.
534 Therefore, in follow up experiments, one can repeat our study but with stabilization, in
535 separate trials, based on the separate eyes (e.g. stabilization in one trial based on right eye
536 motion and stabilization in another trial based on left eye motion). If a particular SC neuron
537 is functionally dominated by input from one eye, then stabilization with one of the eyes
538 should cause larger modulations than stabilization based on the motion of the other eye.

539 This would allow investigating potential ocular dominance of visual information in individual
540 neurons in the awake monkey SC. Moreover, with sufficient mapping across the SC
541 topographic map using such an experiment, it may then be possible to find individual zones
542 in the SC that are potentially dominated (while remaining generally binocular) by visual input
543 from one eye or the other, similar to the finding of orientation tuning zones in the mouse SC
544 [38,39].

546 Since microsaccades are a component of fixational eye movements, it is also likely that they
547 cause similar visual modulations to ocular drifts, but with different spatial and temporal
548 parameters due to the faster and larger nature of microsaccades. This is exactly what we
549 saw recently in the SC [25], and it is also consistent with calculations of the different
550 spatiotemporal consequences of saccades on visual images relative to ocular position drifts
551 [40]. In any case, it is highly unlikely that microsaccades explain our results in the current
552 study, because we excluded these movements from analysis. Also, the microsaccade
553 characteristics were not altered by our retinal image stabilization manipulations but the
554 neural activity was. Therefore, our experiment isolated the effects of the smaller and slower
555 ocular position drifts on SC activity.

557 In all, our results highlight the importance of investigating active vision [41] in the SC [42] and in
558 other visual areas[18,43,44], whether by careful analysis of the image consequences of eye
559 movements on the retina with stable targets (as in Fig. 7) or by experimentally altering the
560 normal visual-motor loop by gaze-contingent manipulation (as in Fig. 3). This would be even
561 more important by using rich visual stimuli – like gratings, textures, and patterns – and even
562 natural images.
563
564
565

Acknowledgements

Author contributions

CYC and ZMH collected the data. ZMH and FK analyzed the data. ZMH wrote the manuscript. ZMH, CYC, and FK edited the manuscript.

Declaration of interests

The authors declare no competing interests.

References

1. Cynader, M., and Berman, N. (1972). Receptive-field organization of monkey superior colliculus. J Neurophysiol 35, 187-201.

2. Goldberg, M.E., and Wurtz, R.H. (1972). Activity of superior colliculus in behaving monkey. I. Visual receptive fields of single neurons. J Neurophysiol 35, 542-559.

3. Chen, C.Y., Hoffmann, K.P., Distler, C., and Hafed, Z.M. (2019). The Foveal Visual Representation of the Primate Superior Colliculus. Curr Biol 29, 2109-2119 e2107. 10.1016/j.cub.2019.05.040.

4. Tailby, C., Cheong, S.K., Pietersen, A.N., Solomon, S.G., and Martin, P.R. (2012). Colour and pattern selectivity of receptive fields in superior colliculus of marmoset monkeys. J Physiol-London 590, 4061-4077. 10.1113/jphysiol.2012.230409.

5. Chen, C.Y., Sonnenberg, L., Weller, S., Witschel, T., and Hafed, Z.M. (2018). Spatial frequency sensitivity in macaque midbrain. Nat Commun 9, 2852. 10.1038/s41467-018-05302-5.

6. Bogadhi, A.R., and Hafed, Z.M. (2022). Express detection and discrimination of visual objects by primate superior colliculus neurons. BioRxiv. 10.1101/2022.02.08.479583.

7. White, B.J., Berg, D.J., Kan, J.Y., Marino, R.A., Itti, L., and Munoz, D.P. (2017). Superior colliculus neurons encode a visual saliency map during free viewing of natural dynamic video. Nat Commun 8, 14263. 10.1038/ncomms14263.

8. Robinson, D.A. (1972). Eye movements evoked by collicular stimulation in the alert monkey. Vision Res 12, 1795-1808. 0042-6989(72)90070-3 [pii].

9. Hafed, Z.M., and Chen, C.Y. (2016). Sharper, Stronger, Faster Upper Visual Field Representation in Primate Superior Colliculus. Curr Biol 26, 1647-1658. 10.1016/j.cub.2016.04.059.

10. Adler, f., and Fliegelman, m. (1934). Influence of fixation on the visual acuity. Archives of Ophthalmology 12, 475-483.

11. Barlow, H.B. (1952). Eye movements during fixation. J Physiol 116, 290-306.

12. Krauskopf, J., Cornsweet, T.N., and Riggs, L.A. (1960). Analysis of eye movements during monocular and binocular fixation. J Opt Soc Am 50, 572-578. 10.1364/josa.50.000572.

13. Rucci, M., Iovin, R., Poletti, M., and Santini, F. (2007). Miniature eye movements enhance fine spatial detail. Nature 447, 851-854. nature05866 [pii] 10.1038/nature05866.

14. Kuang, X., Poletti, M., Victor, J.D., and Rucci, M. (2012). Temporal encoding of spatial information during active visual fixation. Current biology : CB 22, 510-514. 10.1016/j.cub.2012.01.050.

15. Rucci, M., and Victor, J.D. (2015). The unsteady eye: an information-processing stage, not a bug. Trends Neurosci. 10.1016/j.tins.2015.01.005.

16. Ahissar, E., and Arieli, A. (2001). Figuring space by time. Neuron 32, 185-201. 10.1016/s0896-6273(01)00466-4.

17. Gur, M., and Snodderly, D.M. (1987). Studying striate cortex neurons in behaving monkeys: benefits of image stabilization. Vision Res 27, 2081-2087. 0042-6989(87)90122-2 [pii].

18. Segal, I.Y., Giladi, C., Gedalin, M., Rucci, M., Ben-Tov, M., Kushinsky, Y., Mokeichev, A., and Segev, R. (2015). Decorrelation of retinal response to natural scenes by fixational eye movements. Proc Natl Acad Sci U S A. 10.1073/pnas.1412059112.

631 19. Tian, X., Yoshida, M., and Hafed, Z.M. (2016). A Microsaccadic Account of Attentional
632   Capture and Inhibition of Return in Posner Cueing. Frontiers in systems neuroscience
633   *10*, 23. 10.3389/fnsys.2016.00023.
634 20. Tian, X., Yoshida, M., and Hafed, Z.M. (2018). Dynamics of fixational eye position and
635   microsaccades during spatial cueing: the case of express microsaccades. J
636   Neurophysiol *119*, 1962-1980. 10.1152/jn.00752.2017.
637 21. Cherici, C., Kuang, X., Poletti, M., and Rucci, M. (2012). Precision of sustained fixation
638   in trained and untrained observers. Journal of vision *12*. 10.1167/12.6.31.
639 22. Engbert, R., and Kliegl, R. (2004). Microsaccades keep the eyes' balance during
640   fixation. Psychol Sci *15*, 431-436. 10.1111/j.0956-7976.2004.00697.x
641 PSCI697 [pii].
642 23. Snodderly, D.M., Kagan, I., and Gur, M. (2001). Selective activation of visual cortex
643   neurons by fixational eye movements: implications for neural coding. Vis Neurosci
644   *18*, 259-277.
645 24. Tang, Y., Saul, A., Gur, M., Goei, S., Wong, E., Ersoy, B., and Snodderly, D.M. (2007).
646   Eye position compensation improves estimates of response magnitude and receptive
647   field geometry in alert monkeys. J Neurophysiol *97*, 3439-3448. 00881.2006 [pii]
648 10.1152/jn.00881.2006.
649 25. Khademi, F., Chen, C.-Y., and Hafed, Z.M. (2020). Visual feature tuning of superior
650   colliculus neural reafferent responses after fixational microsaccades. Journal of
651   Neurophysiology *123*, 2136-2153. 10.1152/jn.00077.2020.
652 26. Chen, C.Y., and Hafed, Z.M. (2018). Orientation and Contrast Tuning Properties and
653   Temporal Flicker Fusion Characteristics of Primate Superior Colliculus Neurons. Front
654   Neural Circuits *12*, 58. 10.3389/fncir.2018.00058.
655 27. Maior, R.S., Hori, E., Barros, M., Teixeira, D.S., Tavares, M.C., Ono, T., Nishijo, H., and
656   Tomaz, C. (2011). Superior colliculus lesions impair threat responsiveness in infant
657   capuchin monkeys. Neurosci Lett *504*, 257-260. 10.1016/j.neulet.2011.09.042.
658 28. Nguyen, M.N., Matsumoto, J., Hori, E., Maior, R.S., Tomaz, C., Tran, A.H., Ono, T., and
659   Nishijo, H. (2014). Neuronal responses to face-like and facial stimuli in the monkey
660   superior colliculus. Front Behav Neurosci *8*, 85. 10.3389/fnbeh.2014.00085.
661 29. Nguyen, M.N., Nishimaru, H., Matsumoto, J., Van Le, Q., Hori, E., Maior, R.S., Tomaz,
662   C., Ono, T., and Nishijo, H. (2016). Population Coding of Facial Information in the
663   Monkey Superior Colliculus and Pulvinar. Front Neurosci *10*, 583.
664   10.3389/fnins.2016.00583.
665 30. Le, Q.V., Le, Q.V., Nishimaru, H., Matsumoto, J., Takamura, Y., Hori, E., Maior, R.S.,
666   Tomaz, C., Ono, T., and Nishijo, H. (2020). A Prototypical Template for Rapid Face
667   Detection Is Embedded in the Monkey Superior Colliculus. Frontiers in systems
668   neuroscience *14*, 5. 10.3389/fnsys.2020.00005.
669 31. Ahissar, E., and Arieli, A. (2012). Seeing via Miniature Eye Movements: A Dynamic
670   Hypothesis for Vision. Frontiers in computational neuroscience *6*, 89.
671   10.3389/fncom.2012.00089.
672 32. Poletti, M., Aytekin, M., and Rucci, M. (2015). Head-Eye Coordination at a
673   Microscopic Scale. Curr Biol *25*, 3253-3259. 10.1016/j.cub.2015.11.004.
674 33. Skinner, J., Buonocore, A., and Hafed, Z.M. (2019). Transfer function of the rhesus
675   macaque oculomotor system for small-amplitude slow motion trajectories. J
676   Neurophysiol *121*, 513-529. 10.1152/jn.00437.2018.
677 34. Intoy, J., and Rucci, M. (2020). Finely tuned eye movements enhance visual acuity.
678   Nat Commun *11*, 795. 10.1038/s41467-020-14616-2.

679 35. Hubel, D.H., LeVay, S., and Wiesel, T.N. (1975). Mode of termination of retinotectal
680   fibers in macaque monkey: an autoradiographic study. Brain Res *96*, 25-40.
681 36. Pollack, J.G., and Hickey, T.L. (1979). The distribution of retino-collicular axon
682   terminals in rhesus monkey. J Comp Neurol *185*, 587-602. 10.1002/cne.901850402.
683 37. Schiller, P.H., Stryker, M., Cynader, M., and Berman, N. (1974). Response
684   characteristics of single cells in the monkey superior colliculus following ablation or
685   cooling of visual cortex. J Neurophysiol *37*, 181-194. 10.1152/jn.1974.37.1.181.
686 38. Ahmadlou, M., and Heimel, J.A. (2015). Preference for concentric orientations in the
687   mouse superior colliculus. Nat Commun *6*, 6773. 10.1038/ncomms7773.
688 39. Feinberg, E.H., and Meister, M. (2015). Orientation columns in the mouse superior
689   colliculus. Nature *519*, 229-232. 10.1038/nature14103.
690 40. Mostofi, N., Zhao, Z., Intoy, J., Boi, M., Victor, J.D., and Rucci, M. (2020).
691   Spatiotemporal Content of Saccade Transients. Curr Biol *30*, 3999-4008 e3992.
692   10.1016/j.cub.2020.07.085.
693 41. Rolfs, M., and Schweitzer, R. (2022). Coupling perception to action through incidental
694   sensory consequences of motor behaviour. Nat Rev Psychol *1*, 112-123.
695   10.1038/s44159-021-00015-x.
696 42. Hafed, Z.M., Chen, C.Y., Tian, X., Baumann, M., and Zhang, T. (2021). Active vision at
697   the foveal scale in the primate superior colliculus. J Neurophysiol.
698   10.1152/jn.00724.2020.
699 43. Greschner, M., Bongard, M., Rujan, P., and Ammermuller, J. (2002). Retinal ganglion
700   cell synchronization by fixational eye movements improves feature estimation. Nat
701   Neurosci *5*, 341-347. 10.1038/nn821.
702 44. Kagan, I., Gur, M., and Snodderly, D.M. (2008). Saccades and drifts differentially
703   modulate neuronal activity in V1: effects of retinal image motion, position, and
704   extraretinal influences. J Vis *8*, 19 11-25. 10.1167/8.14.19
705 /8/14/19/ [pii].
706 45. Chen, C.Y., Ignashchenkova, A., Thier, P., and Hafed, Z.M. (2015). Neuronal Response
707   Gain Enhancement prior to Microsaccades. Curr Biol *25*, 2065-2074.
708   10.1016/j.cub.2015.06.022.
709 46. Chen, C.Y., and Hafed, Z.M. (2013). Postmicrosaccadic enhancement of slow eye
710   movements. The Journal of neuroscience : the official journal of the Society for
711   Neuroscience *33*, 5375-5386. 10.1523/JNEUROSCI.3703-12.2013.
712 47. Brainard, D.H. (1997). The Psychophysics Toolbox. Spatial vision *10*, 433-436.
713 48. Pelli, D.G. (1997). The VideoToolbox software for visual psychophysics: transforming
714   numbers into movies. Spatial vision *10*, 437-442.
715 49. Kleiner, M., Brainard, D., and Pelli, D.G. (2007). What's new in Psychtoolbox-3?
716   (Abstract). Perception *36*.
717 50. Hafed, Z.M., and Ignashchenkova, A. (2013). On the dissociation between
718   microsaccade rate and direction after peripheral cues: microsaccadic inhibition
719   revisited. J Neurosci *33*, 16220-16235. 10.1523/JNEUROSCI.2240-13.2013.
720 51. Fuchs, A.F., and Robinson, D.A. (1966). A method for measuring horizontal and
721   vertical eye movement chronically in the monkey. J Appl Physiol *21*, 1068-1070.
722 52. Judge, S.J., Richmond, B.J., and Chu, F.C. (1980). Implantation of magnetic search
723   coils for measurement of eye position: an improved method. Vision Res *20*, 535-538.
724 53. Chen, C.Y., and Hafed, Z.M. (2017). A neural locus for spatial-frequency specific
725   saccadic suppression in visual-motor neurons of the primate superior colliculus. J
726   Neurophysiol *117*, 1657-1673. 10.1152/jn.00911.2016.

727   54.   Buonocore, A., Tian, X., Khademi, F., and Hafed, Z.M. (2021). Instantaneous
728   movement-unrelated midbrain activity modifies ongoing eye movements. eLife *10*.
729   10.7554/eLife.64150.
730   55.   Santini, F., Redner, G., Iovin, R., and Rucci, M. (2007). EyeRIS: a general-purpose
731   system for eye-movement-contingent display control. Behav Res Methods *39*, 350-
732   364.
733   56.   Poletti, M., and Rucci, M. (2010). Eye movements under various conditions of image
734   fading. J Vis *10*, 6 1-18. 10.1167/10.3.6
735   /10/3/6/ [pii].
736   57.   Bellet, M.E., Bellet, J., Nienborg, H., Hafed, Z.M., and Berens, P. (2019). Human-level
737   saccade detection performance using deep neural networks. J Neurophysiol *121*,
738   646-661. 10.1152/jn.00601.2018.
739   58.   Zuber, B.L., Stark, L., and Cook, G. (1965). Microsaccades and the velocity-amplitude
740   relationship for saccadic eye movements. Science *150*, 1459-1460.
741   59.   Hafed, Z.M., Goffart, L., and Krauzlis, R.J. (2009). A neural mechanism for
742   microsaccade generation in the primate superior colliculus. Science *323*, 940-943.
743   323/5916/940 [pii]
744   10.1126/science.1166112.
745   60.   Willeke, K.F., Tian, X., Buonocore, A., Bellet, J., Ramirez-Cardenas, A., and Hafed, Z.M.
746   (2019). Memory-guided microsaccades. Nat Commun *10*, 3710. 10.1038/s41467-019-
747   11711-x.
748   61.   Engbert, R., and Kliegl, R. (2003). Microsaccades uncover the orientation of covert
749   attention. Vision Res *43*, 1035-1045. S0042698903000841 [pii].
750   62.   Hafed, Z.M., Lovejoy, L.P., and Krauzlis, R.J. (2011). Modulation of microsaccades in
751   monkey during a covert visual attention task. Journal of Neuroscience *31*, 15219-
752   15230. 10.1523/JNEUROSCI.3106-11.2011.
753
754

Methods

Experimental animals and ethics approvals

We recorded superior colliculus (SC) neural activity from two adult, male rhesus macaque monkeys (N and P) aged 7 years, and weighing 8 kg and 7 kg, respectively. The experiments were approved by ethics committees at the regional governmental offices of the city of Tübingen.

Laboratory setup and animal preparation

The experiments were conducted in the same laboratory as that described in earlier publications [3,9,45]. Briefly, the monkeys were seated in a darkened booth approximately 45 cm from a calibrated and linearized CRT display spanning approximately +/-22 deg horizontally and +/-15 deg vertically. Data acquisition and stimulus control were managed by a custom-made, real-time computing system [19,46], interfacing with the Psychophysics Toolbox [47-49] and a Multi-Channel Acquisition Processor (MAP) data acquisition device (Plexon, Inc.).

The monkeys were prepared for behavioral training and electrophysiological recordings earlier [46,50]. Specifically, each monkey was implanted with a head-holder and scleral search coil in one eye [46]. The search coil allowed tracking eye movements using the magnetic induction technique [51,52], and the head-holder comfortably stabilized head position during the experiments. The monkeys also each had a recording chamber centered on the midline and tilted 38 deg (monkey P) or 35 deg (monkey N) posterior of vertical, allowing access to both the right and left SC [45].

Behavioral task

We employed a gaze fixation task in which we presented static gabor gratings of different spatial frequencies within the receptive fields (RF's) of the recorded neurons. Unlike in our earlier work with spatial frequency mapping in the SC [5,53], we maintained the stimulus on the display for much longer during fixation [54]. Specifically, once we identified the size and location of an RF, we designed a gabor of suitable size to fill the RF. The grating always had high contrast (100%) and one of three different spatial frequencies (0.56, 2.22, or 4.44 cpd), which were varied across trials (the phase of the gabor was also random from trial to trial).

A trial started with the onset of a central white fixation dot over a gray background. After the monkey fixated the spot in a stable manner for a random interval spanning a few hundred milliseconds, the grating appeared in the RF and remained on for approximately 1500 ms. The fixation spot was small (8.5 x 8.5 min arc), and it had a luminance of 72 cd/m^2. The gray background had 21 cd/m^2 luminance. If the monkey successfully fixated the spot for the entire duration of the trial, it was rewarded with fruit juice, and another trial was initiated after a short blank-screen interval.

Four different trial types were interleaved. In the control condition, both the fixation spot and grating were stable on the display. This condition was analyzed for microsaccade-induced visual reafferent responses in a recent study [25], as well as for interactions between spiking activity and microsaccade kinematics [54]. The sustained firing rates during

21

803 microsaccade-free fixation, as well as all the remaining three trial types of the task, were
804 never described in any other publications. The additional trial types constituted our retinal
805 image stabilization manipulations (Fig. 1). In full retinal image stabilization (Fig. 1C), the
806 grating (from the moment it appeared until trial end) was moved in lockstep with
807 instantaneous eye position (see next section). The fixation spot always remained stable on
808 the display to help anchor gaze properly and not alter the eye movement statistics (Figs. S1-
809 S3). This was necessary because we wanted to isolate the influences of (slow) fixational eye
810 movements on neural activity and, therefore, had to ensure that the eye movements
811 themselves were occurring as naturally as possible. In horizontal retinal image stabilization
812 (Fig. 1D), the vertical position of the grating was kept constant on the display and unchanged
813 from control; the horizontal position of the grating was moved in lockstep with horizontal
814 eye position. Finally, in vertical retinal image stabilization (Fig. 1E), the horizontal position of
815 the grating was stable on the display and similar to the control condition, whereas the
816 vertical position of the grating was moved in synchrony with vertical eye position.

818 In a subset of experiments, we replaced the vertical gratings with horizontal ones, in order
819 to explore the relative relationship between eye movement directions and image pattern
820 orientations (e.g. Fig. 4).

822 We collected approximately 18 trial repetitions per condition per neuron.

Retinal image stabilization

826 We first calibrated eye position measurements using methods described earlier [19]. Briefly, at
827 the beginning of every session, the monkeys fixated (multiple times) a series of 19 locations
828 on the display for at least 1000 ms. We then measured raw voltages during stable fixation
829 from each location. To convert the raw voltages to degrees of angular rotation, we used a
830 multi-order polynomial including both the horizontal and vertical raw voltages, as well as
831 cross-channel interaction terms [19].

833 We then employed our real-time gaze-contingent display system [19,20,46]. In this system, we
834 sampled and processed eye positions at 1 KHz using a real-time control system, and we
835 updated the display at 120 Hz (constrained by the display technology). In retinal image
836 stabilization trials, after every display refresh time, we sampled new eye positions and
837 processed them. We then calculated the position of the grating according to the new eye
838 positions, and we updated the display at the next frame refresh. Thus, our retinal image
839 stabilization trials discretized eye positions at 120 Hz (the bottleneck imposed by the display
840 refresh rate). Such a rate is suitable for successful retinal image stabilization with slow eye
841 movements, as shown previously by our [19,20] and other [13,17,55,56] laboratories. In fact, even
842 with microsaccades, Fig. S5 shows that the microsaccade-related reafferent responses were
843 reduced by retinal image stabilization at 120 Hz. This means that while the microsaccades
844 were still a bit too rapid for the display's 120 Hz frequency, the stimulus was still moved
845 sufficiently rapidly to catch up with the real microsaccade and reduce the retinal slip of the
846 grating by the eye movement (and, therefore, the associated reafferent response).

848 Finally, eye coil systems often exhibit a slow drift in their measurements, which is much
849 slower than ocular position drifts (we confirmed this by comparing initial fixation positions
850 across trials and assessing a time constant of eye coil system drift, which was more than two

22

851   orders of magnitude slower than within-trial ocular position drifts). Therefore, at the
852   beginning of every trial, we performed a drift correction that was applied for all subsequent
853   eye position measurements within a trial. We did this by averaging eye position in the final
854   50 ms before gabor onset and using this measurement as a reference to which we compared
855   all subsequent eye positions in the trial. In post-hoc analyses, if there was a microsaccade in
856   the drift correction measurement interval, the trial was excluded from further analysis.
857
858

859   *Eye movement data analysis*
860   We detected saccades and microsaccades as described previously [25,46,57]. We used the
861   detections for two primary purposes. First, we established that microsaccade properties
862   were not altered by our retinal image stabilization manipulations (Fig. S2). Second, for our
863   neural analyses, we excluded all data starting from 10 ms before microsaccade onset until 90
864   ms after microsaccade end. This was done in order to avoid movement-induced reafferent
865   responses from the analyses (Fig. S5). We also inspected all trials for blinks, and we removed
866   all blink intervals, including a period of 50 ms before and a period of 50 ms after each of
867   them.
868

869   Our microsaccade analyses (Fig. S2) included microsaccade rate, directions, and main
870   sequence [58] relationship between movement amplitude and peak velocity. For microsaccade
871   rate, we used a running window of 25 ms width and moved in steps of 2 ms. Within each
872   such time window, we counted the fraction of trials in which the window contained
873   microsaccades across trials of a given condition. For microsaccade directions and main
874   sequence relationships, we considered all microsaccades in the sustained fixation interval
875   that we were interested in for our neural analyses (>300 ms after stimulus onset; see *Neural*
876   *data analysis* below), and we plotted the distribution of movement vector angles (for the
877   direction analysis) or the scatter of movement peak velocity versus movement radial
878   amplitude (for the main sequence analysis). We performed all of these analyses separately
879   for each of the four stimulus conditions (control and three retinal image stabilization
880   versions), and we then compared the results to confirm that retinal image stabilization did
881   not significantly alter the statistics of microsaccades.
882

883   To confirm that retinal image stabilization also did not alter absolute eye position (i.e. the
884   combination of ocular position drifts and microsaccades), we also plotted the raw eye
885   positions (in sustained fixation; >300 ms after stimulus onset) across all trials in each
886   condition (Fig. S1).
887

888   We also analyzed ocular position drifts more specifically. For example, for Fig. S3C-F, we first
889   excluded all microsaccades and their pre- and post-movement periods mentioned above.
890   We then considered all sustained fixation intervals starting from 300 ms after stimulus onset
891   in each trial. For every interval in between two successive microsaccades (which we called a
892   saccade-free fixation interval), we measured mean eye position and subtracted it from every
893   sample of eye position within the same interval. This gave us the instantaneous deviation of
894   eye position from the mean position during the particular saccade-free interval of interest.
895   In Fig. S3C, E, we then binned all such deviations across all fixation intervals and obtained a
896   distribution of how much ocular position drifts altered eye position. For Fig. S3D, F, we also
897   took the standard deviation of eye position within each microsaccade-free fixation interval.
898   We then plotted the distribution of these measurements across all such intervals in Fig. S3D,

23

F. Our purpose in both cases was to highlight that the slow ocular position drifts had similar characteristics whether we ran control or retinal image stabilization trials (Fig. S3C-F), and also to predict the amounts of luminance modulations over the retina that were expected from our gratings and ocular position drift amplitudes (Fig. S3A, B).

Neural data analysis

We recorded from 61 individually isolated SC neurons, which were first characterized online using delayed visually-guided and memory-guided saccade tasks [9,45,53]. The initial characterization allowed classifying the neurons as being visual or visual-motor, as well as assessing the neurons' RF sizes and locations. After establishing that a recorded neuron was visually-responsive, we ran the main behavioral task described above with the grating placed at the optimal RF position (except for some test examples like in Fig. S4). We included all visually-responsive neurons in our analyses, without further classification into visual or visual-motor categories. This was because our results were similar regardless of whether a neuron was purely visual or visual-motor in nature (the results were also highly consistent across the population; for example, Fig. S6A, B).

In both monkeys, we tested the neurons with vertical gratings. In monkey N, we additionally tested 35 neurons with horizontal gratings (27 of these neurons had both vertical and horizontal gratings tested together within the same session).

We analyzed neural data by counting spikes during the sustained fixation interval or by converting spike times into firing rate estimates (with a Gaussian convolution kernel of σ 40 ms). We defined the sustained fixation interval as the time from 300 ms to 1400 ms after grating onset. The lower bound of this time interval (300 ms) was chosen to avoid the initial visual onset response of the neurons (occurring immediately after grating onset); the upper bound was chosen to maximize the numbers of neurons that we could pool in the analyses. We did not notice a difference in the onset response strength (the initial visual burst after grating onset) across our different retinal image stabilization manipulations relative to control. Therefore, we did not analyze initial visual responses further. Rather, we were interested in assessing how subtle image displacements (i.e. during sustained presence of a stimulus within the RF's) affected SC neural activity. Our chosen interval of more than 1 second (300 ms to 1400 ms from stimulus onset) was sufficient to do that.

As stated above, in all of our analyses, except for Fig. S5, we excluded all neural activity associated with microsaccades, in order to avoid contamination by microsaccade-induced reafferent responses [25] (Fig. S5 shows an example of such responses). We replaced all intervals starting from 10 ms before microsaccade onset to 90 ms after microsaccade end by not-a-number labels such that these intervals were not included when computing across-trial averages of firing rates or when computing inter-spike intervals. Note that all of our neurons were not microsaccade-related in the sense of emitting a motor burst at movement onset; they, therefore, did not exhibit prolonged buildup of discharge up to 100 ms before microsaccade onset [59,60]. This justified our choice of pre-microsaccadic mask interval (also see Fig. S5A).

For summarizing population firing rates (e.g. Fig. 3A), we first calculated the within-neuron average firing rate across trial repetitions of a given spatial frequency in the control

24

947   condition. We then normalized each trial's firing rate (for the same spatial frequency) by
948   dividing the trial's instantaneous firing rate (at any given time after stimulus onset) by the
949   peak of the average firing rate in the first 150 ms after stimulus onset. That is, we
950   normalized each trial's firing rate to the peak average firing rate occurring in the early
951   stimulus-evoked visual burst interval of the control condition. We repeated this trial-by-trial
952   normalization procedure for all control trials of the same spatial frequency, and also for all
953   trials of the retinal image stabilization conditions (again of the same spatial frequency). Thus,
954   if a retinal image stabilization condition (e.g. full retinal image stabilization) elevated firing
955   rates relative to control, then the normalized firing rates were also elevated. With all trials
956   and all spatial frequencies normalized to each neuron's response in the respective control
957   condition, we could then average normalized trials across neurons to get population firing
958   rates like in Fig. 3A. This allowed us to visualize the neural modulation effects of retinal
959   image stabilization, and to do further individual neuron and population analyses.
960
961   Among such analyses, we calculated neural modulation indices (e.g. Fig. 3B). To do so, we
962   measured raw firing rates at the individual neuron level across conditions. For each trial of a
963   given spatial frequency, we evaluated the average sustained firing rate (300 ms to 1400 ms
964   after stimulus onset, and with microsaccades removed as per the procedure described
965   above). We did this in the control condition, and we averaged all measurements across trial
966   repetitions ($fr_{control}$). We then repeated this procedure for one of our retinal image
967   stabilization manipulations (full, horizontal, or vertical retinal image stabilization) to obtain
968   $fr_{stabilization}$ (the average within-neuron sustained firing rate during retinal image
969   stabilization). Then, we calculated a modulation index comparing retinal image stabilization
970   to control as: $(fr_{stabilization} - fr_{control})/(fr_{stabilization} + fr_{control})$; that is, the modulation index was the
971   average sustained firing rate in a retinal image stabilization manipulation minus the average
972   sustained firing rate in the control condition, divided by the sum of the two measurements.
973
974   We plotted histograms of modulation indices across the entire population of neurons, with
975   indications of the average modulation index across neurons (e.g. pink vertical line in Fig. 3B).
976   We tested whether the population modulation indices were significantly different from zero
977   using a t-test and reported p-values in the figures and/or text. In the Results text, we also
978   often reported the average modulation index values as percentages by multiplying the
979   values from the calculation above by 100. We also often compared neural modulation
980   indices across conditions (e.g. comparing the effects of retinal image stabilization for high or
981   low spatial frequency gratings). We did so by performing a t-test across the different
982   conditions and reporting p-values.
983
984   For scatter plots of individual neuron results, we followed similar procedures to those above
985   for the modulation indices. For example, in Fig. S6A, we counted the number of spikes per
986   trial in the sustained interval (i.e. per 1100 ms occurring between 300 ms and 1400 ms after
987   stimulus onset) in either the control condition or the full retinal image stabilization
988   condition. This resulted in a paired measurement per neuron (average spike count per
989   control trial and average spike count per retinal image stabilization trial). We then plotted all
990   of these measurements across the population as a scatter plot. Note that microsaccades
991   were still excluded in such analyses, exactly as above. However, since microsaccade
992   characteristics were unchanged across conditions (Fig. S2), the microsaccade exclusion was
993   not inappropriately favoring one condition over the other when comparing the spike counts
994   across them. Therefore, it was appropriate to exclude the occasionally occurring rapid eye

995   movements in this manner. Also note that the spike counts in these kinds of analyses were
996   essentially estimates of average sustained firing rates. This is so because such spike counts
997   were evaluated over an interval of approximately 1 second duration (1100 ms).
998
999   We also computed inter-spike intervals during sustained fixation in either control or one of
1000 the retinal image stabilization manipulations (e.g. Fig. S6C). Because we excluded
1001 microsaccades, there could be intervals within trials that were replaced with not-a-number
1002 labels during the exclusion process. Therefore, for inter-spike interval measurements, we
1003 first found contiguous blocks of fixation data within trials that existed in between successive
1004 microsaccades. Then, we computed inter-spike intervals within all such contiguous blocks.
1005 This allowed us to avoid counting inter-spike intervals during (and around) microsaccades,
1006 and also to avoid having erroneously large inter-spike intervals due to the not-a-number
1007 labels introduced during preprocessing (e.g. if we had counted two spikes on either side of a
1008 not-a-number block of data).
1009
1010 For summarizing microsaccade-induced reafferent responses at the individual neuron level
1011 in Fig. S5B, we used a similar procedure to our earlier analyses (e.g. Fig. S6A). The only
1012 difference is that our measurement interval was now different. Here, for each microsaccade
1013 in a given condition, we measured the firing rate in the interval 30-80 ms after microsaccade
1014 onset (see gray bar on the x-axis in Fig. S5A). This interval captured the reafferent response.
1015 We then compared, within each neuron, the average response with and without retinal
1016 image stabilization (Fig. S5B).
1017
1018 For some of our analyses, we selected neurons according to their preferred eccentricities or
1019 visual field locations. For example, we categorized neurons based on whether they were
1020 foveal or extrafoveal (Fig. 6); or whether they were part of the upper or lower visual field
1021 representation of the SC (Figs. S10, S11). To do so, we classified neurons according to the
1022 eccentricity and direction from horizontal of their RF hotspots (Fig. S9).
1023
1024 Finally, for Fig. 7, our goal was to ask whether horizontal or vertical ocular position drifts in
1025 control trials were still sufficient to modulate SC neural responses in a manner that was
1026 consistent with the retinal image stabilization results. For every control trial of a given
1027 spatial frequency, we had a moving window of 250 ms duration (starting from 300 ms after
1028 stimulus onset and in steps of 1 ms). If the window was devoid of microsaccades (including
1029 the pre- and post-microsaccadic masks described above) and the eye position was within +/-
1030 3 min arc (horizontally and vertically) from the initial fixation position, we measured eye
1031 position variability (horizontal or vertical) in the first 200 ms of the interval and firing rate in
1032 the final 50 ms of the interval. That is, we assumed that SC neurons integrate the recent
1033 history (200 ms) of the image over the RF's in their instantaneous firing rate. This was
1034 justified based on prior measurements of the temporal properties of SC neurons [26]. Our
1035 measure of variability was the standard deviation of eye position during the interval. We
1036 then did a median split based on this variability across all microsaccade-free epochs of a
1037 given neuron, and we compared firing rates for high or low variability trials. We did this
1038 independently for horizontal and vertical variability. Thus, for vertical gratings, we could
1039 compare epochs with high variability of horizontal eye position (orthogonal to the grating) to
1040 epochs with low variability of horizontal eye position. If our retinal image stabilization results
1041 were indeed related to the image luminance modulations of orthogonal eye position shifts,
1042 then such comparison would yield a difference between high and low horizontal drift

1043   variability. Similarly, if we now compared epochs of low and high vertical eye position
1044   variability, we would have expected no neural effects (analogous to parallel retinal image
1045   stabilization). We did this procedure for all neurons and across different spatial frequencies.
1046
1047
1048
1049
1050

Supplementary figures
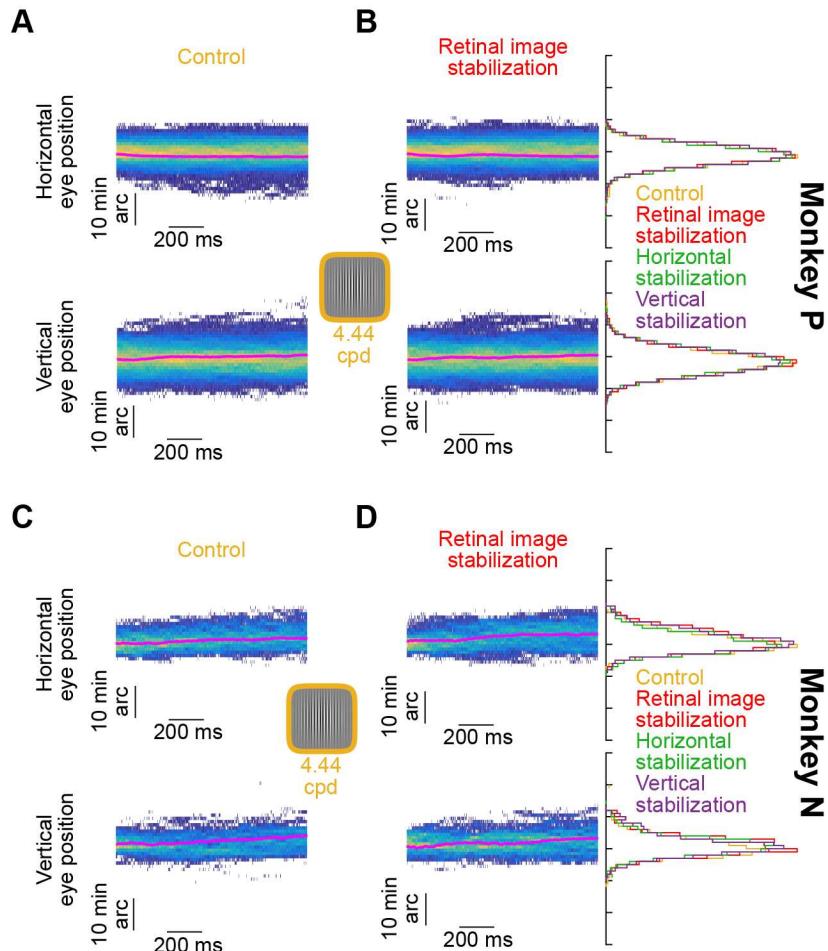
Figure S1 Similarity of fixational eye positions during retinal image stabilization and control trials. (A) Histograms of raw horizontal (top) and vertical (bottom) eye positions from monkey P as a function of time from stimulus onset, in the interval from 300 ms to 1400 ms (control trials with a 4.44 cpd gabor grating are shown). The thick pink line in each histogram is the mean eye position. **(B)** Same as **A** but for full retinal image stabilization. The marginal histograms on the right show the distributions of eye positions (across all times) for the control condition, the retinal image stabilization condition (red), as well as the two other retinal image stabilization conditions of Fig. 1D, E. The distributions of eye positions were similar across all conditions, suggesting that retinal image stabilization did not alter eye movement characteristics in our experiments (Methods). **(C, D)** Same as **A**, **B** but for monkey N. The same results were observed in both monkeys for the low (0.56 cpd) and intermediate (2.22 cpd) spatial frequency trials.
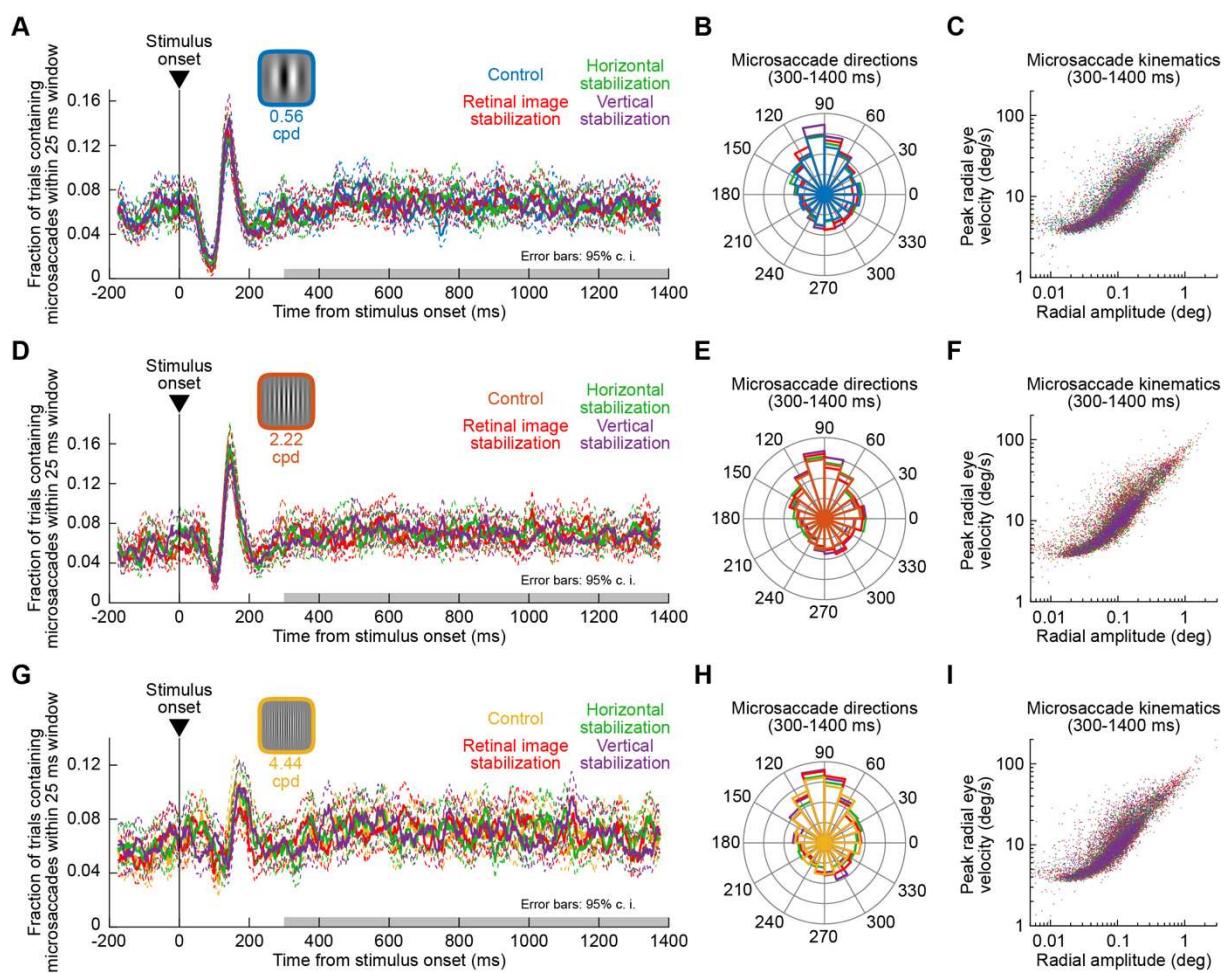
28

1069

1070
1071
1072 **Figure S2 Similarity of microsaccade characteristics between control trials and all retinal image stabilization**
1073 **trials. (A)** Microsaccade rate (+/- 95% confidence intervals) as a function of time from stimulus onset from all
1074 trials with a 0.56 cpd grating (monkey P shown as an example). The different colors show the different conditions
1075 (control plus the three retinal image stabilization conditions of Fig. 1C-E). Initially, microsaccade rate was
1076 modulated by stimulus onset, as expected [50,61,62], and was then stable. Critically, the modulations in
1077 microsaccades were similar across all of our experimental conditions (control versus the three types of retinal
1078 image stabilization). The gray bar denotes our analysis interval for exploring the influences of microsaccade-free
1079 ocular position drifts on SC neural activity. **(B, C)** Microsaccade directions **(B)** and kinematics **(C)** during sustained
1080 fixation were also unaltered by retinal image stabilization. **(D-F)** Same as **A-C**, but for the trials in which a 2.22
1081 cpd grating was presented. **(G-I)** Same as **A-C**, but for 4.44 cpd trials. Monkey N showed the same results of no
1082 impact of retinal image stabilization on microsaccade characteristics. Note that in all of our neural analyses
1083 (except for Fig. S5), we excluded all microsaccades as well as pre- and post-movement intervals around them
1084 before taking any measurements (Methods). Our purpose in the current analysis was merely to demonstrate
1085 that the properties of microsaccades (like drifts in Fig. S1) were largely unaffected by the retinal image
1086 stabilization technique. This was due to the stability of the fixation spot on the display.
1087

1088
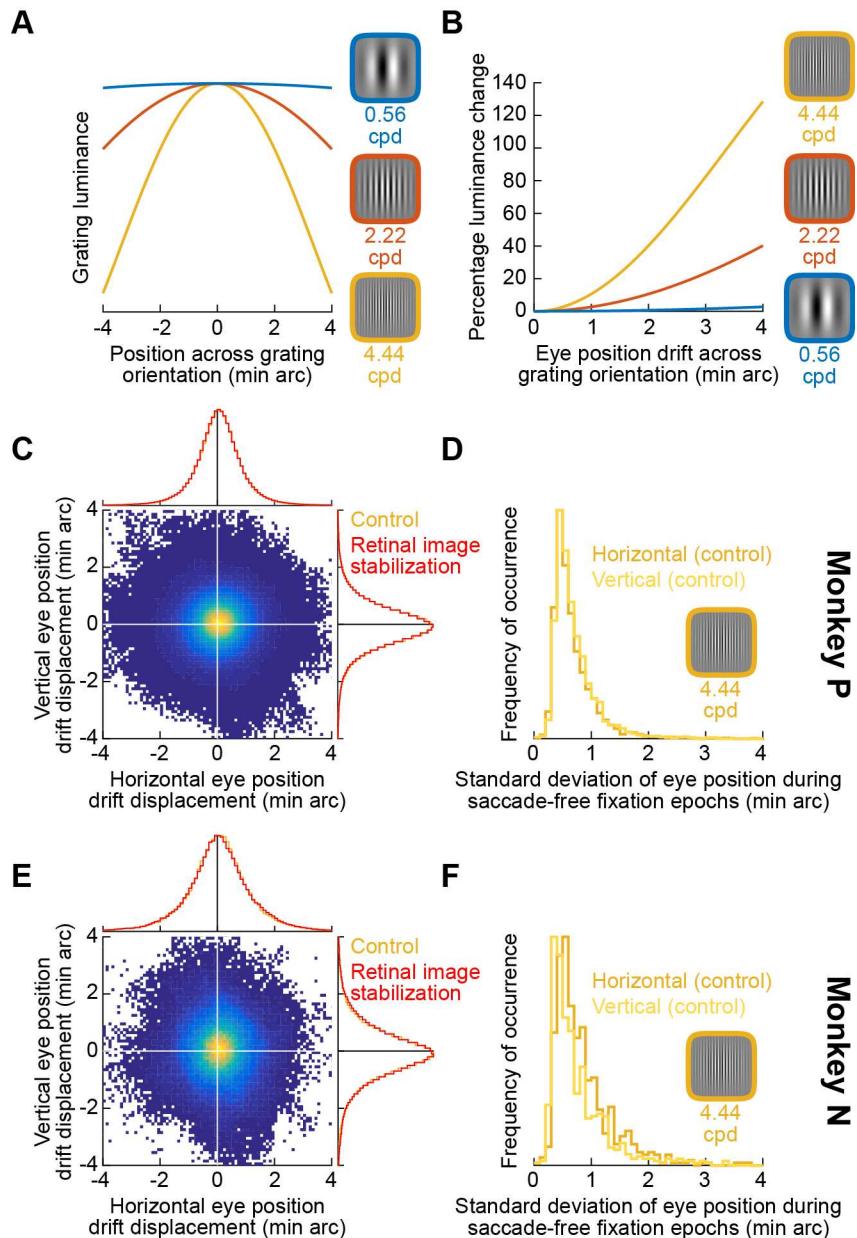
1089
1090
1091 **Figure S3 Spatial scale of the image pattern displacements over SC neurons' visual RF's. (A)** Luminance profile
1092 of each of our three tested spatial frequencies as a function of position orthogonal to the grating orientation. **(B)**
1093 Ocular position drifts on the scale of 1 min arc are associated with the highest instantaneous change in luminance
1094 experienced at a given retinotopic location for the highest spatial frequency grating. **(C)** Two dimensional
1095 histogram of naturally-occurring displacements of eye position during microsaccade-free fixation. Within any
1096 microsaccade-free epoch, we measured the range of eye position deviation from mean position during the epoch
1097 (Methods). We did this for the control condition from one of our trial types (4.44 cpd trials), but the results were
1098 the same across all conditions (see Figs. S1, S2). The horizontal/vertical yellow histograms show the marginal
1099 distributions in each direction; the red histograms overlaid on top show the same distributions from the full
1100 retinal image stabilization condition for comparison. Microsaccade-free fixation epochs were associated with
1101 displacements on the order of 1 min arc, and were unchanged by our gaze-contingent manipulation (compare
1102 red and yellow histograms). **(D)** Variability estimate of microsaccade-free eye position drifts in monkey P (retinal
1103 image stabilization conditions yielded similar histograms). **(E, F)** Similar observations in monkey N. Natural
1104 fixation behavior in both monkeys was expected to cause predictable luminance modulations of image patterns
1105 over SC receptive fields, and such behavior was unchanged by our experimental manipulations (see Figs. S1, S2).
1106

1107
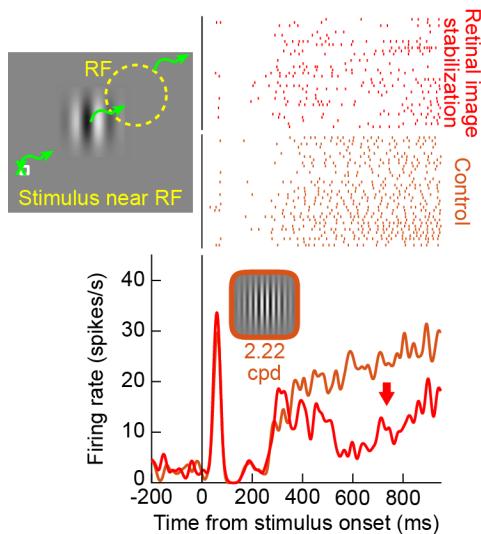
1108
1109
1110 **Figure S4 Validating the retinal image stabilization technique by forcing a grating position at a sub-optimal RF**
1111 **position (away from RF center).** The schematic shows the experimental manipulation that we applied for this
1112 neuron. We presented a grating stimulus displaced away from the preferred RF location indicated by the dashed
1113 yellow circle. Therefore, the stimulus was near the RF, but at a sub-optimal position. Forcing this position during
1114 retinal image stabilization significantly reduced the sustained response of the neuron. This is the complement of
1115 the example neuron results shown in Fig. 2, in which forcing a stimulus at the best receptive field location
1116 elevated the neural response relative to control.
1117
1118
1119

1120
1121
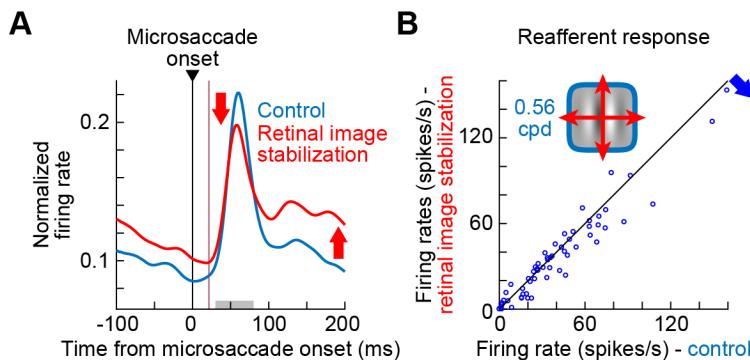
1122
1123

1124 **Figure S5 Validating the retinal image stabilization technique by exploring SC visual reafferent responses after**
1125 **microsaccades [25]. (A)** Across all neurons, we plotted normalized firing rate (as in Fig. 3A), but this time by aligning
1126 data to microsaccades during sustained fixation (as opposed to during microsaccade-free fixation, as in Fig. 3).
1127 We did this for presentations of a 0.56 cpd vertical grating. In control trials, there was an expected visual
1128 reafferent response immediately after microsaccades [25]. With retinal image stabilization, firing rate was elevated
1129 long before and long after microsaccades (consistent with our main results like in Figs. 2, 3). However, the
1130 reafferent response was reduced relative to control. This is because, even though microsaccades were fast
1131 relative to display updates, the retinal image stabilization technique still partially tracked these rapid eye
1132 movements. This resulted in subdued retinal-image motion caused by the microsaccades (relative to the control
1133 condition). Such a reduction in microsaccade-induced retinal-image motion is known to reduce the SC visual
1134 reafferent response [25]. **(B)** Across all neurons, we measured the microsaccade-induced reafferent response
1135 (during the gray interval on the x-axis in **A**) in the control and retinal image stabilization trials (Methods). There
1136 was a consistent reduction in the reafferent response during retinal image stabilization (p=0.0015; 2-sample t-
1137 test; n=61 neurons). Higher spatial frequency gratings had significantly weaker reafferent responses even during
1138 control trials [25], making the effects of retinal image stabilization harder to observe.
1139

1140
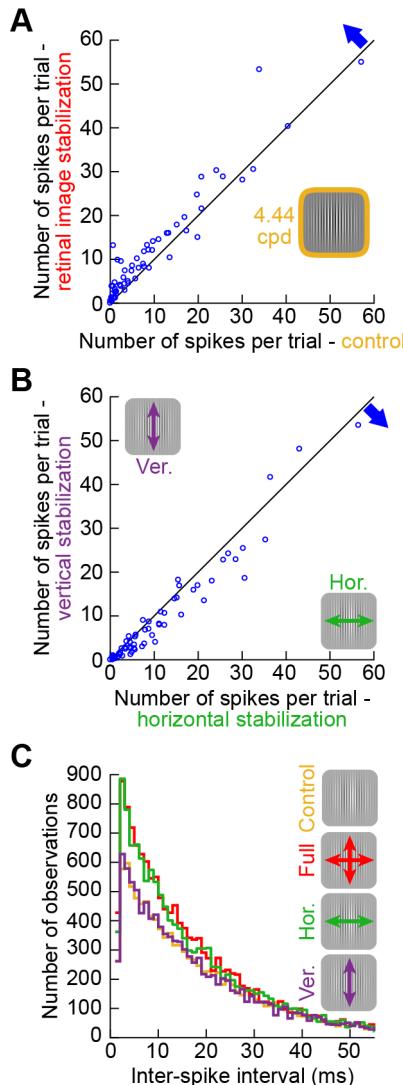
1141
1142
1143 **Figure S6 Individual neuron results from Fig. 3. (A)** We measured raw neural activity during sustained fixation
1144 (excluding peri-microsaccadic intervals; Methods) for the analyses of Fig. 3A, B. The x-axis counts the number of
1145 spikes per trial in control, and the y-axis counts the number of spikes per trial in retinal image stabilization. Note
1146 that given the length of our measurement interval (gray region on the x-axis in Fig. 3A), the shown values of spike
1147 counts are quantitatively equivalent to the approximate sustained firing rate of the neurons during the trials.
1148 Also, note that since microsaccade characteristics were unaltered by retinal image stabilization (Fig. S2), the
1149 shown differences in firing rates across the conditions could not be attributed to potentially different
1150 distributions of microsaccades across image stabilization manipulations. Rather, there was a consistent elevation
1151 of sustained neural activity (blue arrow) by retinal image stabilization (p=1.436x10^{-5}; 2-sample t-test; n=61
1152 neurons). This is consistent with the results of Fig. 3A, B. **(B)** We also compared the individual neuron spike counts
1153 across the horizontal and vertical retinal image stabilization conditions (as in Fig. 3C-F). The neurons consistently
1154 exhibited elevated activity for horizontal (orthogonal) rather than vertical retinal image stabilization
1155 (p=3.142x10^{-6}; 2-sample t-test; n=61 neurons). **(C)** Across all neurons, inter-spike interval distributions reflected
1156 the results of Fig. 3: horizontal and full retinal image stabilization resulted in more SC activity than in control
1157 trials, but vertical retinal image stabilization did not. The inter-spike interval distributions also reveal that the SC
1158 spiking statistics (e.g. burstiness) were not significantly altered by retinal image stabilization.
1159

33

1160
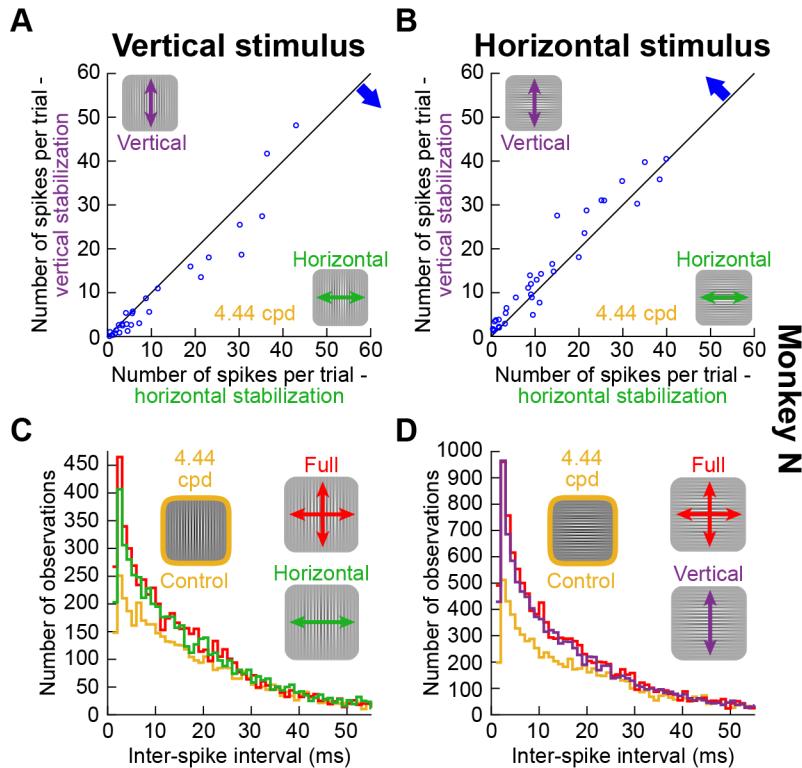
1161
1162
1163 **Figure S7 Individual neuron results with horizontal gratings showed similar results to the main experiments**
1164 **with vertical gratings. (A)** Same as Fig. S6B but from the monkey in which we also collected horizontal grating
1165 trials. The same results as in Fig. S6B were observed, as expected (p=0.0072). **(B)** In the same animal, when we
1166 flipped the image pattern from vertical to horizontal, it was now vertical retinal image stabilization trials that
1167 resulted in elevated firing rates relative to horizontal retinal image stabilization trials (p=0.0026; 2-sample t-
1168 test; n=35 neurons). Therefore, it was the relative (orthogonal) relationship between the image pattern and the
1169 stabilization direction that mattered for the neurons, consistent with Figs. 4, S8. **(C, D)** Similar to Fig. S6C but
1170 for vertical (**C**) or horizontal (**D**) gratings in the same animal. Note that with horizontal gratings (**D**), it was now
1171 vertical retinal image stabilization that resulted in indistinguishable results from full retinal image stabilization
1172 (instead of horizontal retinal image stabilization as in the case of vertical gratings in **C**).
1173

1174
1175
1176
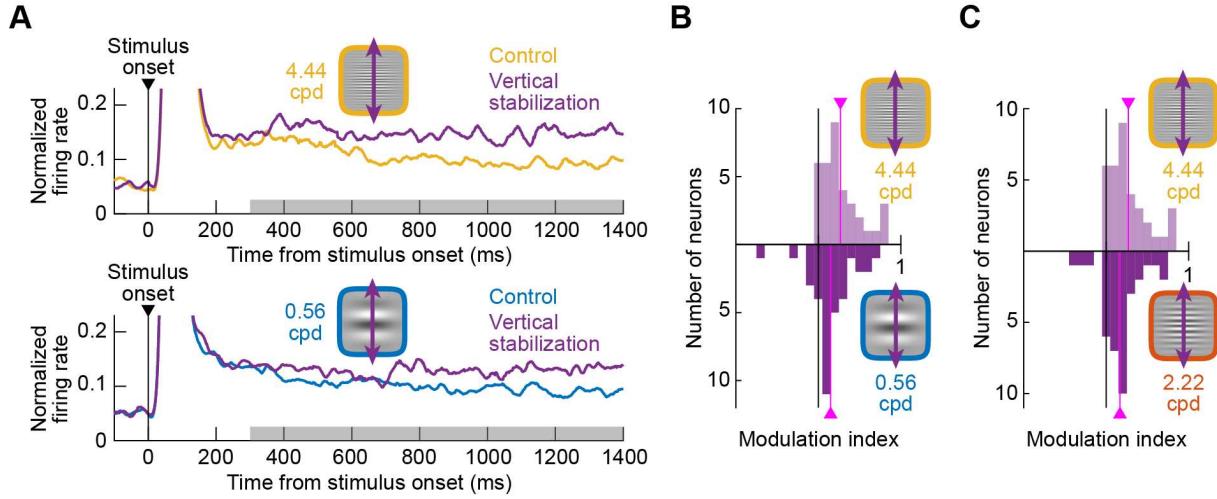
1177
1178
1179 **Figure S8 Dependence of neural modulation on spatial frequency even with horizontal gratings. (A)** Similar to
1180 Fig. 5A but for horizontal gratings and vertical retinal image stabilization (Fig. 4 showed that vertical retinal
1181 image stabilization with horizontal gratings was equivalent to horizontal retinal image stabilization with vertical
1182 gratings due to the orthogonal relationship between eye movements and image patterns in both cases). There
1183 was a higher modulation of neural activity by the retinal image stabilization technique for high (top) than low
1184 (bottom) spatial frequencies (compare each stabilization curve to its respective control curve), consistent with
1185 Fig. 5. **(B)** Similar to Fig. 5B but for horizontal gratings with vertical retinal image stabilization. The population
1186 average modulation indices were 26.84% and 14.94% for 4.44 cpd and 0.56 cpd gratings, respectively
1187 (p=0.0529; 2-sample t-test; n=35 neurons). **(C)** Similar to Fig. 5C but for horizontal gratings and vertical retinal
1188 image stabilization. Similar results to **B** were now obtained when comparing 4.44 cpd (26.84% average
1189 modulation index) to 2.22 cpd (16.76% average modulation index; p=0.0845 comparing 4.44 cpd to 2.22 cpd
1190 modulations; 2-sample t-test; n=35 neurons). Therefore, with both vertical (Fig. 5) and horizontal (this figure)
1191 gratings, the same dependence of neural activity on the relative spatial scale of image patterns and ocular
1192 position drifts was observed.
1193
1194

35

1195
1196
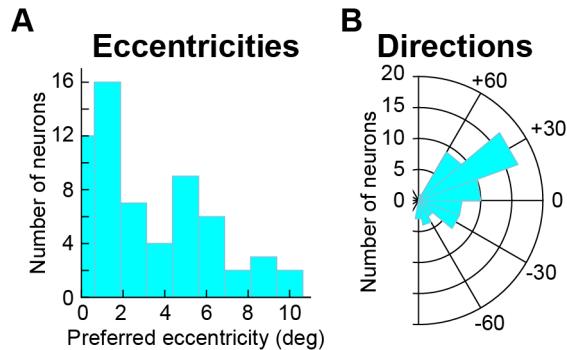
Figure S9 RF hotspot locations of the recorded neurons. (A) Distribution of preferred eccentricities by our neurons. We sampled foveal and extrafoveal neurons. **(B)** Distribution of the directions of the RF hotspot locations relative to the horizontal meridian. We sampled both upper and lower visual field neurons.

1197
1198
1199
1200
1201
1202

1203
1204
1205
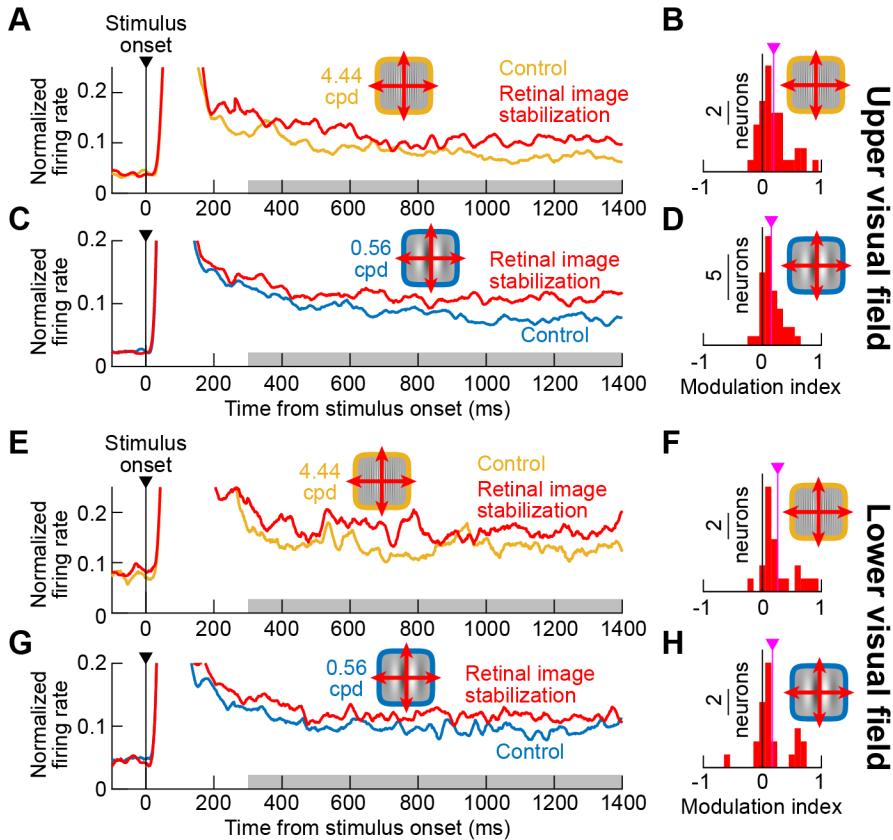
1206
1207

Figure S10 Sensitivity of both upper and lower visual field SC neurons to the visual-pattern consequences of ocular position drifts on the scale of 1 min arc amplitude. (A) Normalized firing rates in control and retinal image stabilization from all neurons with RF hotspots occupying the upper visual field. A 4.44 cpd vertical grating was presented to the neurons. As in Fig. 3, neural activity was systematically elevated with retinal image stabilization. **(B)** Modulation indices for the individual neurons in **A**. There was a significant positive modulation across the population (average modulation of 19.2% across the population; pink vertical line; $p=4.009\times10^{-5}$; 1-sample t-test; n=37 neurons). **(C, D)** Same as **A**, **B** but for a low spatial frequency grating. The average modulation index was now 15.13% ($p=1.649\times10^{-6}$; 1-sample t-test; n=37 neurons). **(E-H)** Same as **A**-**D** but for lower visual field SC neurons, which we showed earlier (in the same animals) to have significantly larger RF's than upper visual field neurons [9]. There was still significant positive elevation of neural activity for these neurons ($p=2.94\times10^{-4}$ for **F** and $p=0.0134$ for **H**). Therefore, even SC neurons with relatively large RF's are still sensitive to the visual-pattern consequences of ocular position drifts.

1208
1209
1210
1211
1212
1213
1214
1215
1216
1217
1218
1219
1220

1221
1222
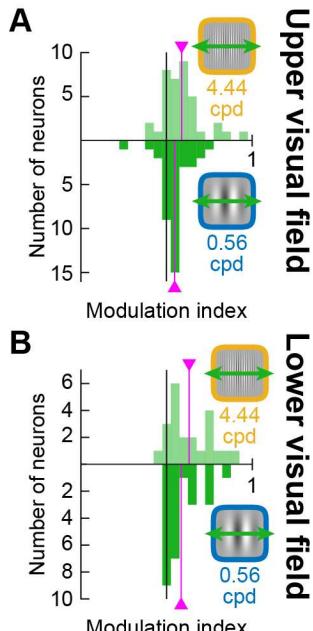
1223
1224
1225 **Figure S11 Ocular position drifts cause stronger modulations with high spatial frequency patterns than low**
1226 **spatial frequency patterns in both upper and lower visual field SC neurons. (A)** Similar analyses to Fig. 5 but
1227 only for upper visual field neurons. The average modulation indices (pink vertical lines) for high and low spatial
1228 frequencies were 17.61% and 9.49%, respectively (p=0.0481; 2-sample t-test comparing high to low populations;
1229 n=37 neurons). **(B)** Same as **A** but for lower visual field neurons with larger RF's. The modulation indices were
1230 now 26.33% and 17.03% for high and low spatial frequencies, respectively (p=0.0066; 2-sample t-test comparing
1231 high to low spatial frequency populations; n=24 neurons). Similar results were obtained with full retinal image
1232 stabilization, as expected.
1233
1234